1 **Global Soil Consumption of Atmospheric Carbon Monoxide:**

2 **An Analysis Using a Process-Based Biogeochemistry Model**

3 Licheng Liu[1], Qianlai Zhuang[1,2], Qing Zhu[1,3], Shaoqing Liu[1,4], Hella van Asperen[5], Mari

4 Pihlatie[6,7]

[1]Department of Earth, Atmospheric, Planetary Sciences, Purdue University, West Lafayette, IN 47907, USA

[2]Department of Agronomy, Purdue University, West Lafayette, IN 47907, USA

[3] Climate Sciences Department, Climate & Ecosystem Sciences Division, Lawrence Berkeley National Laboratory, Berkeley, CA 94720, USA

[4]Department of Earth Sciences, University of Minnesota, Minneapolis, MN, 55455,USA

[5]Institute of Environmental Physics, University of Bremen, Otto-Hahn-Allee 1, Bremen, 28359, Germany

[6]Department of Physics, University of Helsinki, P.O. Box 48, 00014 University of Helsinki, Finland

[7]Department of Forest Sciences, P.O. Box27, 00014 University of Helsinki, Finland

5 *Correspondence to:* Qianlai Zhuang(qzhuang@purdue.edu)

Abstract: Carbon monoxide (CO) plays an important role in controlling the oxidizing capacity of the atmosphere by reacting with OH radicals that affect atmospheric methane (CH_4) dynamics. We develop a process-based biogeochemistry model to quantify CO exchange between soils and the atmosphere with a 5-minute internal time step at the global scale. The model is parameterized using CO flux data from the field and laboratory experiments for eleven representative ecosystem types. The model is then extrapolated to the global terrestrial ecosystems using monthly climate forcing data. Global soil gross consumption, gross production, and net flux of the atmospheric CO are estimated to be from -180 to -197, 34 to 36, and -145 to -163 Tg CO yr^{-1} (1Tg = 10^{12} g), respectively, driven with satellite-based atmospheric CO concentration data during 2000-2013. Tropical evergreen forest, savanna and deciduous forest areas are the largest sinks at 123 Tg CO yr^{-1}. Soil CO gross consumption is sensitive to air temperature and atmospheric CO concentration while gross production is sensitive to soil organic carbon (SOC) stock and air temperature. By assuming that the spatially-distributed atmospheric CO concentrations (~128 ppbv) are not changing over time, global mean CO deposition velocity is estimated to be 0.16-0.19 mm s^{-1} during the 20th century. Under the future climate scenarios, the CO deposition velocity will increase at 0.0002-0.0013 mm s^{-1} yr^{-1} during 2014-2100, reaching 0.20-0.30 mm s^{-1} by the end of the 21st century. Areas near the equator, Eastern US, Europe and eastern Asia will be the largest sinks due to optimum soil moisture and high temperature. The annual global soil net flux of atmospheric CO is primarily controlled by air temperature, soil temperature, SOC and atmospheric CO concentrations, while its monthly variation is mainly determined by air temperature, precipitation, soil temperature and soil moisture.

1. Introduction

Carbon monoxide (CO) plays an important role in controlling the oxidizing capacity of the atmosphere by reacting with OH radicals (Logan et al., 1981; Crutzen, 1987; Khalil & Rasmussen, 1990; Prather et al., 1995; Prather & Ehhalt, 2001). CO in the atmosphere can directly and indirectly influence the fate of critical greenhouse gases such as methane (CH_4) and ozone (O_3) (Tan and Zhuang, 2012). Although CO itself absorbs only a limited amount of infrared radiation from the Earth, the cumulative

39 indirect radiative forcing of CO may be even larger than that of the third powerful

40 greenhouse gas, nitrous oxide (N_2O, Myhre et al., 2013). Current estimates of global

41 CO emissions from both anthropogenic and natural sources range from 1550 to 2900

42 Tg CO yr^{-1}, which are mainly from anthropogenic and natural direct emissions and from

43 the oxidation of methane and other Volatile Organic Compounds (VOC) (Prather et al.,

44 1995; Khalil et al., 1999; Bergamaschi et al., 2000; Prather & Ehhalt, 2001, Stein et al.,

45 2014). Chemical consumption of CO by atmospheric OH and the biological consumption

46 of CO by soil microbes are two major sinks of the atmospheric CO (Conrad, 1988; Lu &

47 Khalil, 1993; Yonemura et al., 2000; Whalen & Reeburgh, 2001).

48   Soils are globally considered as a major sink for CO due to microbial activities

49 (Whalen and Reeburgh, 2001; King and Weber, 2007). A diverse group of soil microbes

50 including carboxydotrophs, methanotrophs and nitrifiers are capable of oxidizing CO

51 (King and Weber, 2007). Annually, 10-25% of total earth surface CO emissions were

52 consumed by soils (Sanhueza et al., 1998; King, 1999a; Chan & Steudler, 2006). Potter

53 et al. (1996) reported the global soil consumption to be from -16 to -50 Tg CO yr^{-1}

54 (positive values represent the emissions from soils to the atmosphere), by using a

55 single-box model over the upper 5 cm of soils. All existing estimates have large

56 uncertainties ranging from -16 to -640 Tg CO yr^{-1} (Sanhueza et al., 1998; King, 1999;

57 Bergamaschi et al., 2000). Similarly, the estimates of CO dry deposition velocities also

58 have large uncertainties, ranging from 0 to 4.0mm s^{-1} (here positive values are amount

59 of deposition to soils, King, 1999a; Castellanos et al., 2011). Soils also produce CO

60 mainly via abiotic processes such as thermal- and photo-degradation of organic matter

61 or plant materials (Conrad and Seiler, 1985b; Tarr et al., 1995; Schade et al., 1999;

62 Derendorp et al., 2011; Lee et al., 2012; van Asperen et al., 2015; Fraser et al., 2015,

63 Pihlatie et al., 2016), except for a few cases of anaerobic formation. Photo-degradation

64 is identified as radiation-dependent degradation due to absorbing radiation (King et al.,

65 2012). Thermal-degradation is identified as the temperature-dependent degradation of

66 carbon in the absence of radiation and possibly oxygen (Derendorp et al., 2011; Lee et

67 al., 2012; van Asperen et al., 2015; Pihlatie et al., 2016). These major soil CO

68 production processes, together with soil CO consumption processes, have not been

69 adequately modeled in global soil CO budget estimates.

To date, most top-down atmospheric models applied a dry deposition scheme based on the resistance model of Wesely (1989). Such schemes provided a wide range of dry deposition velocities (Stevenson et al., 2006). Only a few models (MOZART-4, Emmons et al., 2010; CAM-chem, Lamarque et al., 2012) have extended their dry deposition schemes with a parameterization for CO and H_2 uptake through oxidation by soil microbes following the work of Sanderson et al. (2003), which itself was based on extensive measurements from Yonemura et al. (2000). Potter et al. (1996) developed a bottom-up model to simulate CO consumption and production at the global scale. This model is a single box model, only considers top 5cm depth of soil and does not have explicit microbial factors, which might have underestimated CO consumption (Potter et al., 1996; King, 1999a). Current bottom-up CO modeling approaches are mostly based on a limited number of CO *in situ* observations or laboratory studies to quantify regional and global soil consumption (Potter et al., 1996; Sanhueza et al., 1998; Khalil et al., 1999; King, 1999a; Bergamaschi et al., 2000; Prather & Ehhalt, 2001). To our knowledge, no detailed process-based model of soil-atmospheric exchange of CO has been published in the recent 15 years. One reason is that there is an incomplete understanding of biological processes of uptake (King & Weber, 2007; Vreman et al., 2011; He and He, 2014; Pihlatie et al., 2016). Another reason is that there is lack of long-term CO flux measurements for different ecosystem types to calibrate and evaluate the models. CO flux measurements are mostly from short-term field observations or laboratory experiments (e.g. Conrad and Seiler, 1985a; Funk et al., 1994; Tarr et al., 1995; Zepp et al., 1997; Kuhlbusch et al., 1998; Moxley and Smith, 1998; Schade et al., 1999; King and Crosby, 2002; Varella et al., 2004; Lee et al., 2012; Bruhn et al., 2013; van Asperen et al., 2015). The first study to report long-term and continuous field measurements of CO flux over grasslands using a micrometeorological eddy covariance (EC) method is Pihlatie et al. (2016).

To improve the quantification of the global soil CO budget for the period 2000-2013 and CO deposition velocity for the 20th and 21st centuries, this study developed a CO dynamics module (CODM) embedded in a process-based biogeochemistry model, the Terrestrial Ecosystem Model (TEM) (Zhuang et al., 2003, 2004, 2007). CODM was then calibrated and evaluated using laboratory experiments and field measurements for

different ecosystem types. The atmospheric CO concentration data from MOPITT (Gille, 2013) were used to drive model simulations from 2000 to 2013. A set of century-long simulations of 1901-2100 were also conducted using the atmospheric CO concentrations estimated with an empirical function (Badr & Probert, 1994; Potter et al., 1996). Finally, the effects of multiple forcings on the global CO consumption and production, including the changes of climate and atmospheric CO concentrations at the global scale were evaluated with the model.

2. Method

2.1 Overview

We first developed a daily soil CO dynamics module (CODM) that considers: (1) soil-atmosphere CO exchange and diffusion process between soil layers, (2) consumption by soil microbial oxidation, (3) production by soil chemical oxidation, and (4) the effects of temperature, soil moisture, soil CO substrate and surface atmospheric CO concentration on these processes. Second, we used the observed soil temperature and moisture to evaluate TEM hydrology module and soil thermal module in order to estimate soil physical variables. Then we used the data from laboratory experiments and CO flux measurements to parameterize the model using the Shuffled Complex Evolution (SCE-UA) method (Duan et al., 1993). Finally, the model was extrapolated to the globe at a 0.5° by 0.5° resolution. We conducted three sets of model experiments to investigate the impact of climate and atmospheric CO concentrations on soil CO dynamics: 1) simulations for 2000-2013 with MOPITT satellite atmospheric CO concentration data; 2)simulations for 1901-2100 with constant atmospheric CO concentrations estimated from an empirical function and the historical climate data (1901-2013) and three future climate scenarios (2014-2100); and 3) Eight sensitivity simulations by changing a) constant CO surface concentrations ± 30%, b) SOC ±30%, c) precipitation ±20% and d) air temperature ± 3°C for each pixel, respectively, while holding other forcing data as they were, during 1999-2000.

2.2 Carbon Monoxide Dynamics Module (CODM)

131   Embedded in TEM (Figure 1), CODM is mainly driven by: (1) soil organic carbon

132   availability based on a carbon and nitrogen dynamics module (CNDM) (Zhuang et al.,

133   2003); (2) soil temperature profile from a soil thermal module (STM) (Zhuang et al.,

134   2001, 2003); and (3) soil moisture profile from a hydrological module (HM) (Bonan,

135   1996; Zhuang et al, 2004). Net exchange of CO between the atmosphere and soil is

136   determined by the mass balance approach (net flux = total production – total oxidation –

137   total soil CO concentration change). According to previous studies, we separated active

138   soils (top 30cm) for CO consumption and production into 1 cm thick layers (King, 1999a,

139   1999b; Whalen & Reeburgh, 2001; Chan & Steudler, 2006). Between the soil layers, the

140   changes of CO concentrations were calculated as:

$$141 \qquad \frac{\partial(C(t,i))}{\partial t} = \frac{\partial}{\partial z}\left(D(t,i)\frac{\partial\big(C(t,i)\big)}{\partial z}\right) + P(t,i) - O(t,i) \qquad (1)$$

142   Where $C(t,i)$ is the CO concentration in layer i and at time t, units are mg m^{-3}. z is the

143   depth of the soil, units are m. $D(t,i)$ is the diffusion coefficient for layer i, units are m^2 s^{-1}

144   . $P(t,i)$ is the CO production rate and $O(t,i)$ is the CO consumption rate. The units of

145     $P(t,i)$ and $O(t,i)$ are mg m^{-3} s^{-1}. $D(t,i)$ is calculated using the method from Potter et al.

146   (1996), equations (2) to (4), which are the functions of soil temperature, soil texture and

147   soil moisture. The upper boundary condition is specified as the atmospheric CO

148   concentration, which is estimated by an empirical function of latitude (Potter et al., 1996)

149   or directly measured by the MOPITT satellite during 2000-2013. The lower boundary

150   condition is assumed to have no diffusion exchange with the layer underneath. This

151   partial differential equation (PDE) is solved using the Crank-Nicolson method for less

152   time-step-sensitive solution.

153   CO consumption was modeled in unsaturated soil pores as:

$$154 \qquad O(t,i) = V_{max} \cdot f_1\big(C(t,i)\big) \cdot f_2\big(T(t,i)\big) \cdot f_3\big(M(t,i)\big) \qquad (2)$$

155   Where V_{max} is the specific maximum oxidation rate, ranging from 0.3 to 11.1 µg CO g^{-1}

156   h^{-1} (Whalen & Reeburgh, 2001). f_i represents the effects of soil CO concentration

157     $C(t,i)$, temperature $T(t,i)$ and moisture $M(t,i)$ on CO soil consumption. Considering

158   CO consumption as the result of microbial activities, we calculated $f_1\big(C(t,i)\big)$,

159     $f_2\big(T(t,i)\big)$ and $f_3\big(M(t,i)\big)$ in a similar way as Zhuang et al. (2004):

160
$$f_1\big(C(t,i)\big) = \frac{C(t,i)}{C(t,i) + k_{CO}} \qquad (2.1)$$

161
$$f_2\big(T(t,i)\big) = Q_{10}^{\frac{T(t,i)-T_{ref}}{10}} \qquad (2.2)$$

162
$$f_3\big(M(t,i)\big) = \frac{(M(t,i) - M_{min})(M(t,i) - M_{max})}{(M(t,i) - M_{min})(M(t,i) - M_{max}) - (M(t,i) - M_{opt})^2} \qquad (2.3)$$

163   Where $f_1\big(C(t,i)\big)$ is a multiplier that enhances oxidation rate with increasing soil CO

164   concentrations using a Michaelis-Menten function with a half-saturation constant k_{CO},

165   ranging from 5 to 51 µl CO l^{-1} (Whalen & Reeburgh, 2001); $f_2\big(T(t,i)\big)$ is a multiplier that

166   enhances CO oxidation rates with increasing soil temperature using a Q10 function with

167   Q_{10} coefficients (Whalen & Reeburgh, 2001). T_{ref} is the reference temperature, units

168   are °C (Zhuang et al., 2004, 2013). $f_3\big(M(t,i)\big)$ is a multiplier to estimate the biological

169   limiting effect that diminishes CO oxidation rates if the soil moisture is not at an optimum

170   level (M_{opt}). M_{min}, M_{max} and M_{opt} are the minimum, maximum and optimum volumetric

171   soil moistures of oxidation reaction, respectively. Equation (2.2) will overestimate CO

172   consumption at higher temperature because in reality CO consumption will decrease at

173   higher temperatures than optimum temperature, while f_2 will keep increasing with rising

174   temperature. However, the CO consumption is constrained by CO production, and

175   equation (1) is used to represent this constraint.

176   We modeled the CO production rate ($P(t,i)$) as a process of chemical oxidation

177   constrained by soil organic carbon (SOC) decay (Conrad and Seiler,1985; Potter et al.

178   1996; Jobbagy & Jackson, 2000; van Asperen et al., 2015):

179
$$P(t,i) = P_r(t,i) \cdot E_{SOC} \cdot C_{SOC}(t) \cdot F_{SOC} \qquad (3)$$

180   Where $P_r(t,i)$ is a reference soil CO production rate which has been normalized to rate

181   at reference temperature (production rate at temperature (t,i) divided by production

182   rate at reference temperature), which is affected by soil moisture and soil temperature

183   (Conrad and Seiler,1985; van Asperen et al., 2015). E_{SOC} is an estimated nominal CO

184   production factor of 3.5 ± 0.9 X 10^{-9} mg CO m^{-2} s^{-1} per g SOC m^{-2} (to 30 cm surface soil

185   depth) (Potter et al., 1996). $C_{SOC}(t)$ is a SOC content in mg m^{-2}, which is provided by

186   CNDM module in TEM. F_{SOC} is a constant fraction of top 30cm SOC compared to total

187   amount of SOC, which is 0.33 for shrubland areas, 0.42 for grassland areas and 0.50

188   for forest areas, respectively (Jobbagy & Jackson, 2000). $P_r(t, i)$ was calculated as:

189    $$P_r(t, i) = \exp\left(f_4\big(M(t, i)\big) \cdot Ea_{ref}/R \cdot \left(\frac{1}{273.15 + PT_{ref}} - \frac{1}{T(t, i) + 273.15} \right) \right) \quad (3.1)$$

190    $$f_4\big(M(t, i)\big) = \frac{PM_{ref}}{M(t, i) + PM_{ref}} \quad (3.2)$$

191   Where equation (3.1) is derived from Arrhenius equation for chemical reactions and

192   normalized using the reference temperature PT_{ref}. Ea_{ref}/R is the reference activation

193   energy divided by gas constant R, units are K. $f_4\big(M(t, i)\big)$ is the multiplier that reduces

194   activation energy using a regression approach based on laboratory experiment of

195   moisture influences on CO production (Conrad and Seiler,1985). PM_{ref} is the reference

196   volumetric soil moisture, ranging from 0.01 to 0.5 volume/volume (v/v). We assumed

197   thermal-degradation as the main CO producing process due to lack of photo-

198   degradation data and hard to distinguish photo-degradation from observations. In order

199   to reduce the bias from thermal-degradation to total abiotic degradation, the equation

200   (3.1) is parameterized by comparing with total production rate. For instance, $P_r(t, i)$

201   calculation can perfectly fit the experiment results in Van Asperen et al., 2015 with

202   proper PT_{ref}(18°C), Ea_{ref}/R(14000 K) and PM_{ref}(0.5 v/v).

203   CO deposition velocity was modeled in the same way as equation (19.1) in

204   Seinfeld, et al. (1998):

205    $$v_d = -F_{net}/C_{CO,air} \quad (4)$$

206   Where the v_d is the CO deposition velocity, units are mm s^{-1}; F_{net} is the model

207   estimated CO net flux rate, units are mg CO m^{-2} day^{-1}; $C_{CO,air}$ is the CO surface

208   concentration, units are ppbv. $C_{CO,air}$ can be MOPITT CO surface concentration data or

209   derived CO surface concentrations using the same method as Potter et al. (1996).

210   Positive values of v_d are soil uptakes (depositions from air to soils) and negative values

211   are soil emissions.

212

213   **2.3 Model Parameterization and Extrapolation**

214   The model parameterization was conducted in two steps: 1) Thermal and
215 hydrology modules embedded in TEM were revised, calibrated and evaluated by
216 running model with corresponding local meteorological or climatic data at four
217 representative sites, including boreal forest, temperate forest, tropical forest and
218 savanna (Table 1, site No.1 to 4, Figure 2) to minimize model data mismatch in terms of
219 soil temperature and moisture. 2) CODM module was parameterized by running TEM
220 for observational periods with the corresponding local meteorological or climatic data at
221 each reference site (Table 1, Figure 3), and using the Shuffled Complex Evolution
222 Approach in R language (SCE-UA-R) (Duan et al., 1993) to minimize the difference
223 between simulated and observed net CO flux. Eleven parameters including k_{CO}, V_{max},
224 T_{ref}, Q_{10}, M_{min}, M_{max}, M_{opt}, E_{SOC}, Ea_{ref}/R, PM_{ref} and PT_{ref} were optimized (Table 2). To
225 be noticed, F_{SOC} was not involved in the calibration process. Parameter priors were
226 decided based on previous studies (Conrad & Seiler, 1985; King, 1999b; Whalen &
227 Reeburgh, 2001; Zhuang et al., 2004). SCE-UA-R was used for site No. 6, 8, 10, 11
228 (Table 1). Each site has been run 50 times using SCE-UA-R with 10000 maximum
229 loops for parameter ensemble, and all of them reached stable state before the end of
230 the loops. For wetlands, the only available data is from site No.12. We used a trial-and-
231 error method to make our simulated results in the range of observed flux rates, with a
232 10% tolerance. For tropical sites, since tropical savanna vegetation type is a
233 combination type of tropical forest and grassland in our model, we first used Site No. 13
234 to set priors to fit the experiment results with a 10% tolerance and then evaluated by
235 running our model comparing with site No.7 results. Site No. 9 and 5 were used to
236 evaluate our model results for temperate forest and grassland. Besides the observed
237 climatic and soil property data, we used ERA-Interim reanalysis data from The
238 European Centre for Medium-Range Weather Forecasts (ECMWF) (Dee et al., 2011),
239 AmeriFlux observed meteorology data (http://ameriflux.lbl.gov/) and reanalysis climatic
240 data from Climatic Research Unit (CRU, Harris et al., 2013) to fill the missing
241 environmental data. To sum up, parameters for various ecosystem types in Table 2
242 were the final results of our parameterization. Model parameterization was conducted
243 for ecosystem types including boreal forest, temperate coniferous forest, temperate
244 deciduous forest, and grassland using SCE-UA-R. Tropical forest and wet tundra used

245 a trial-and-error method to adjust parameters letting simulation results best fit the lab
246 data. Due to limited data availability, we assumed temperate evergreen broadleaf forest
247 having the same parameters as temperate deciduous forest.
248

249 **2.4 Data Organization**

250   To get spatially and temporally explicit estimates of CO consumption, production
251 and net flux at the global scale, we used the data of land cover, soils, climate and leaf
252 area index (LAI) from various sources at a spatial resolution of 0.5° latitude X 0.5°
253 longitude to drive TEM. The land cover data include potential vegetation distribution
254 (Melillo et al., 1993) and soil texture (Zhuang et al., 2003), which were used to assign
255 vegetation- and texture-specific parameters to each grid cell.

256   For the simulation of the period 1901-2013, monthly air temperature, precipitation,
257 clouds fraction and vapor pressure data sets from CRU were used to estimate the soil
258 temperature, soil moisture and SOC with TEM (Figure 4). Monthly LAI data from TEM
259 were required to simulate soil moisture (Zhuang et al., 2004). During this period time,
260 we used an empirical function of latitude, which was derived from the observed
261 latitudinal distribution of tropospheric carbon monoxide (Badr and Probert, 1994) to
262 calculate CO surface concentrations (equation (7), Potter et al., 1996):

263 $$C_{CO,air} = 82.267856 + 0.8441503L + 1.55934 \times 10^{-2}L^2 + 2.37 \times 10^{-5}L^3 -$$

264 $$2.3 \times 10^{-6}L^4 \qquad\qquad (5)$$

265   Where $C_{CO,air}$ is the derived surface CO concentration (ppbv), *L* represents
266 latitude which is negative degrees for southern hemisphere and positive degrees for
267 northern hemisphere. We also used the atmospheric CO data from MOPITT satellite
268 during 2000-2013 (Figure 5). We averaged day-time and night-time monthly mean
269 retrieved CO surface level 3 data (variables mapped on 0.5° latitude X 0.5° longitude
270 grid scales with monthly time step, Gille, 2013) to represent the CO surface
271 concentration level in each month. The missing pixels were fixed by the average of
272 pixels which had values and were inside 1.5 times of the distance between this missing
273 pixel and the nearest pixel with values. These global mean values shown in Figure 5 do
274 not include ocean surfaces, thus there are differences between our surface CO

concentration results and Yoon and Pozzer's report in 2014, which is as low as 99.8ppb. From 2014 to 2100, we used Intergovernmental Panel on Climate Change (IPCC) future climate scenarios from Representative Concentration Pathways (RCPs) climate forcing data sets RCP2.6, RCP4.5 and RCP8.5 (Figure 6). RCP2.6, 4.5 and 8.5 datasets are future climate projections with anthropogenic greenhouse gas emission radiative forcing of 2.6 W m^{-2}, 4.5 W m^{-2} and 8.5 W m^{-2}, respectively, by 2100. Since RCPs did not have water vapor pressure data, we used the specific humidity and sea level air pressure from the RCPs and elevation of surface to estimate the monthly surface vapor pressure (Seinfeld & Pandis, 1998).

2.5 Model Experiment Design

We conducted two sets of core simulations and eight sensitivity test simulations for a historical period. The two core sets of simulations were driven with MOPITT CO surface concentrations data for the period 2000-2013 (experiment E1) and with spatially distributed CO surface concentrations assuming as constant over time estimated from an empirical function of latitude for the period 1901-2100 (experiment E2), respectively. Specifically, in experiment E2 we used the CRU climate forcing for the historical period 1901-2013 and the climate data of RCP2.6, RCP4.5 and RCP8.5 for different future scenarios to examine the responses of CO flux to changing climates. Eight sensitivity simulations were driven with varying different forcing variables while keeping others as they were: 1) with constant CO surface concentrations ± 30%, 2) SOC ±30%, 3) precipitation ±20% and 4) air temperature ± 3°C for each pixel, respectively, during 1999-2000 (E3).

3. Results

3.1 Site Evaluation

Both the magnitude and variation of the simulated soil temperature and moisture from cold areas to warm areas compared well to the observations (Figure. 2). The magnitude of the simulated CO flux is comparable and correlated with the observations (r is about 0.5, p-value < 0.001, Figures 3, a2, b2 ,c2 ,d2). Estimated CO fluxes for

305 different ecosystem types range from -28.4 to 1.7 mg CO m^{-2} day^{-1}, and the root mean

306 square error (RMSE) between simulation and observation at all sites is below 1.5 mg

307 CO m^{-2} day^{-1}. RMSE for site No. 7 is bigger than 2.0 mg CO m^{-2} day^{-1} when compared

308 with transparent chamber observations.   For boreal forest site, we only had 8

309 acceptable points in 1994 and 1996 (Figure 3c2).

310

311 **3.2 Global Soil CO Dynamics During 2000-2013**

312   Using the MOPITT CO surface concentration data during 2000-2013 (E1), the

313 estimated mean soil CO consumption, production and net flux (positive values indicate

314 CO emissions from soils to the atmosphere) are from -180 to -197, 34 to 36 and -145 to

315 -163 Tg CO yr^{-1}, respectively (Figure 7a). Consumption is about 4 times larger than

316 production. The annual consumption and net flux trends follow the atmospheric CO

317 concentration trends (Figure 5b, Figure 7a), with a small interannual variability (<10%).

318 The latitudinal distributions of consumption, production and net fluxes share the same

319 spatial pattern. Around 20°S-20°N and 20-60N° are the largest and second largest

320 areas for production and consumption, while the 45°S-45°N area accounts for nearly 90%

321 of the total consumption and production (Figure 7b, Table 3). The Southern and

322 Northern Hemispheres have 41% and 59% of the total consumption, and 47% and 53%

323 of the total production, respectively (Table 3). The highest rates of consumption and

324 production are located in areas close to the equator, and consumption from areas such

325 as eastern US, Europe and eastern Asia also is high (>-1000 mg m^{-2} yr^{-1}) (Figure 8a, b).

326 Global soils serve as an atmospheric CO sink (Figure 8c). Some areas, such as

327 western US and southern Australia, are CO sources, all of which are grasslands or

328 experiencing dry climate. Tropical evergreen forests are the largest sinks, consuming 86

329 Tg CO yr^{-1}, and tropical savanna and deciduous forest are second and third largest

330 sinks, consuming a total of 37 Tg CO yr^{-1} (Table 4). These three ecosystems account

331 for 66% of the total consumption. Tropical evergreen forests are also the largest source

332 of soil CO production, producing 16 Tg CO yr^{-1}, while tropical savanna has a

333 considerable production of 6 Tg CO yr^{-1} (Table 4). Moreover, tropical areas, including

334 forested wetlands, forested floodplain and evergreen forests, are most efficient for CO

335 consumption, ranging from -13 to -18 mg CO m^{-2} $day^{-1.}$ They are also the most efficient

336 for CO production at over 2 mg CO m^{-2} day^{-1} (Table 4, calculated by fluxes divided by

337 area).

338

339 **3.3 Global Soil CO Dynamics During 1901-2100**

340   Using the constant CO surface concentration, the estimated global mean CO

341 deposition velocities are 0.16-0.19 mm s^{-1} for the period 1901-2013. For the period

342 2014-2100, deposition velocities are 0.18-0.21, 0.18-0.24 and 0.17-0.31 for RCP2.6, 4.5

343 and 8.5 scenarios, respectively (Figure 9). During 2014-2100, there are significant

344 trends of increasing consumption, production and net flux for nearly all scenarios

345 (Figure 9). The rates of increasing are 0.0002, 0.0005 and 0.0013 mm s^{-1} yr^{-1}, and will

346 reach 0.20, 0.23 and 0.30 mm s^{-1} by the end of the 21st century for the RCP2.6, 4.5 and

347 8.5 scenarios, respectively (Figure 9). These increasing trends are similar to air

348 temperature increasing trends (Figure 6a). Global distribution patterns of CO deposition

349 velocity are similar to net flux distribution for the period 2000-2013 but there are

350 significant differences among 1901-2013, RCP2.6, RCP4.5 and RCP8.5 scenarios

351 (Figure 10). Deposition velocities are increasing from RCP2.6 to 8.5 and larger than in

352 the historical periods in areas near the equator (Figure 10). Areas near the equator and

353 eastern Asia become big sinks of atmospheric CO, while northeastern US becomes a

354 small source in the 21st century (Figure 10). Different vegetation types have a large

355 range of deposition velocity, from 0.008 to 1.154 mm s^{-1} (Table 5). The tropical forested

356 wetland, tropical forested floodplain and tropical evergreen forest have top three largest

357 deposition velocity of 1.154, 1.117 and 0.879 mm s^{-1}, respectively, while desert, short

358 grasslands, and wet tundra have the smallest deposition velocity 0.008, 0.010 and

359 0.015 mm s^{-1}, respectively.

360

361 **3.4 Sensitivity test**

362   Eight sensitivity tests have been conducted for the 1999-2000 period, including

363 changing atmospheric CO by ±30%, SOC by ±30%, precipitation by ±30% and air

364 temperature by ±3°C for each pixel (Table 5). Soil CO consumption is most sensitive

(changing 29%) to air temperature while production is most sensitive (changing up to 36%) to both air temperature and SOC (30%). The net CO fluxes have the similar sensitivities as consumption. Annual CO consumption, production and net flux follow the change of air temperature (Table 5). In addition, a 30% change in precipitation will not lead to large changes in CO flux (< 3%).

4. Discussion

4.1 Comparison with Other Studies

Previous studies estimated a large range of global CO consumption from -16 to -640 Tg CO yr^{-1}. Our estimates are from -180 to -197 Tg CO yr^{-1} for for 2000-2013 using MOPITT satellite CO surface concentration data. Previous studies also provided a large range for CO production from 0 to 7.6 mg m^{-2} day^{-1} (reviewed in Pihlatie et al., 2016). Our results showed averaged CO production ranging from 0.01 to 2.29 mg m^{-2} day^{-1}. Previously reported CO deposition velocities for different vegetation types range from 0.0 to 4.0 mm s^{-1} while our results showed an averaged CO deposition velocity ranging from 0.006 to 1.154 mm s^{-1} for different vegetation types. The large uncertainty of these estimates is mainly due to a different consideration of the microbial activities, the depth of the soil, and the parameters in the model. In contrast to the estimates of -16 to -57 Tg CO yr^{-1} which were based on top 5 cm soils (Potter et al., 1996), our estimates considered 30cm soils, just as used in Whalen & Reeburgh (2001). In addition, we used a thinner layer division (1cm each layer) for diffusion process, and used the Crank-Nicolson method to solve partial differential equations to avoid time step influences. We also included the microbial CO oxidation process to remove the CO from soils and the effects of soil moisture, soil temperature, vegetation type and soil CO substrate on microbial activities. Our soil thermal, soil hydrology and carbon and nitrogen dynamics simulated in TEM provided carbon substrate spatially and temporally for estimating soil CO dynamics. Overall, although a few previous studies have examined the long-term impacts of climate, land use and nitrogen depositions on CO dynamics (Chan &

393 Steudler, 2006, Pihlatie et al., 2016), the global prediction of soil CO dynamics still has
394 a large uncertainty.

395

396 **4.2 Major Controls to Soil CO Dynamics**

397   Sensitivity tests indicate that consumption is normally much larger than CO
398 production so that the former will determine the dynamics of the net flux (Table 5).
399 Model being sensitive to air temperature explains the small increasing trends after the
400 1960s, the significant increasing trend in the 21st century and the large sinks over
401 tropical areas (Table 5, Figure 9). SOC did not directly influence CO consumption. For
402 instance, increasing SOC led to an increase in soil CO substrate, implying that more CO
403 in soils can be consumed. To be noticed, the CO oxidation increasing due to CO
404 substrate change is larger than production increasing due to SOC increasing, leading to
405 an extra 18 Tg CO yr^{-1} being taken up from the atmosphere to soils in sensitivity test
406 when SOC increasing by 30% (Table 5). CO concentrations will only influence the
407 uptake rate and soil CO substrate concentrations, thus influencing the soil CO
408 consumption rate.

409   Annual CO consumption and net flux have a similar correlation coefficient with
410 forcing variables and both are significantly correlated with air temperature, soil
411 temperature SOC and atmospheric CO concentration (R > 0.91 globally, Table 6).
412 Increasing temperature will increase microbial activities, while more SOC will increase
413 soil CO substrate level. Annual CO consumption and net flux have low correlations with
414 annual precipitation and soil moisture, especially at 45°N-45°S (R<0.54 Table 6).
415 Annual CO production is strongly correlated with annual mean SOC, air temperature
416 and soil temperature (R>0.91), while is less correlated with precipitation, soil moisture
417 and atmospheric CO concentration. Meanwhile, the monthly CO consumption,
418 production and net flux are well correlated with air temperature, soil temperature,
419 precipitation, and soil moisture (R>0.69 globally Table 6). The soil moisture is
420 significantly influenced by temperature at a monthly time step since increasing
421 temperature would induce higher evapotranspiration. Monthly CO consumption,
422 production and net flux have low correlations with SOC because it will not change
423 greatly within a month.

424   The R between annual soil CO consumption and atmospheric CO concentration
425   is 0.91 at the global scale because the atmospheric CO concentration, air temperature,
426   and soil temperature dominate the annual consumption rate. At monthly scale, this R is
427   -0.48 because global atmospheric CO concentrations are high in winter and low in
428   summer while the simulated soil CO consumption shows an opposite monthly variation
429   (Table 6, Figure 11), suggesting that other factors such as precipitation, air temperature,
430   and soil temperature are major controls for monthly CO fluxes.

431

432   **4.3. Model Uncertainties and Limitations**

433   There are a number of limitations, contributing to our simulation uncertainties.
434   First, due to lacking long-period observational data of CO flux and associated
435   environmental factors, the model parameterization can only be conducted for 4
436   ecosystem types including boreal forest, temperate coniferous forest, temperate
437   deciduous forest and grassland. Tropical forest calibration is only conducted using a
438   very limited amount of lab experiment data, but tropical areas are hotspots for CO soil-
439   atmosphere exchanges. Besides, tropical forest SOC for top 30cm can be really high
440   according to observations. TEM model may underestimate the top 30cm SOC, which
441   will underestimate production rates, especially in tropical regions. Tropical regions
442   typically have high temperature during the whole year, which may result in
443   overestimation of CO consumption using equation (2.2). The large deviation for tropical
444   savanna (which is mosaic of tropical forest and grassland ecosystems) may be due to
445   using outside air temperature to represent inside air temperature of transparent
446   chamber observations (Varella et al., 2004), and uncertain tropical forest
447   parameterization. Second, we used the conclusion from van Asperen et al. (2015) and
448   only considered the thermal-degradation process for CO production in this study. Photo-
449   degradation process and biological formation process were not considered due to
450   lacking understanding of these processes. Third, the derived CO surface concentration
451   is lower than MOPITT CO surface concentration, which will lead to overestimation of
452   CO deposition velocity during 1901-2100. Fourth, our model structure still has a large
453   potential to improve. In this study we divided the top 30cm soil into 30 layers (layer
454   thickness dz=1cm), but finer division will increase the accuracy (Figure 12). We chose

455   dz=1cm because if dz>1cm, the model vertical CO concentration profile will deviate

456   from reality and diffusion process will be influenced significantly. If dz<1cm, it will need

457   much more computing time but don't have much improvement compared to dz=1cm

458   (Figure 12a-e). We notice that the 30-layer division well represents soil CO

459   concentration profile not only for the days with soil CO net uptake, but also for the days

460   with CO net emission (Figure 12c, f). Fifth, Michaelis-Menten function (equation 2.1) is

461   used in this model and we notice that k_{CO} is normally much larger than $C(t,i)$ in those

462   days of net soil uptake (over ten times larger, Figure 12). However, we can't simplify

463   equation (2.2) to $f_1\big(C(t,i)\big) = \frac{C(t,i)}{k_{CO}}$ since CO concentrations in soils can be larger than

464   in the atmosphere in the days of net emissions and $C(t,i)$ may be close to k_{CO}, which

465   may lead to overestimation of CO oxidation (Figure 12f). Finally, although we focused

466   on natural ecosystems in this study, land-use change, agriculture activity, and nitrogen

467   deposition also affect the soil CO consumption and production (King, 2002; Chan &

468   Steudler, 2006). For instance, soil CO consumption in agriculture ecosystems is 0 to 9

469   mg CO m^{-2} day^{-1} in Brazil (King & Hungria, 2002). We used grass land or forest

470   ecosystem to represent agriculture areas in CODM module. Our future study shall

471   include these processes and factors.

472

473   **5. Conclusions**

474   We analyzed the magnitude, spatial pattern, and the controlling factors of the

475   atmosphere-soil CO exchanges at the global scale for the 20th and 21st centuries using

476   a process-based biogeochemistry model. Major processes include atmospheric CO

477   diffusion into soils, microbial oxidation removal of CO, and CO production through

478   chemical reaction. We found that air temperature and soil temperature play a dominant

479   role in determining annual soil CO consumption and production while precipitation, air

480   temperature, and soil temperature are the major controls for the monthly consumption

481   and production. Atmospheric CO concentrations are important for annual CO

482   consumption. We estimated that the global annual CO consumption, production and net

483   fluxes for 2000-2013 are from -180 to -197, 34 to 36 and -145 to -163 Tg CO yr^{-1},

484   respectively, when using a MOPITT CO surface concentration data. Tropical evergreen

485   forest, savanna and deciduous forest areas are the largest sinks accounting for 66% of

486   the total CO consumption, while the Northern Hemisphere consumes 59% of the global

487   total. During the 20th century, the estimated CO deposition velocity is 0.16-0.19 mm s^{-1}.

488   The predicted CO deposition velocity will reach 0.20-0.30 mm s^{-1} in the 2090s, primarily

489   because of increasing air temperature. The areas near the equator, eastern Asia,

490   Europe and eastern US will become the sink hotspots because they have warm and

491   moist soils. This study calls for long-period observations of CO flux for various

492   ecosystem types and projection of atmospheric CO surface concentrations from 1901-

493   2100 to improve future estimates of global soil CO consumption. The effects of land-use

494   change, agriculture activities, nitrogen deposition, photo-degradation and biological

495   formation shall also be considered to improve future quantification of soil CO fluxes.

496

497

498 **Acknowledgment**

499   This study is supported through projects funded to Q.Z. by Department of Energy

500   (DE-SC0008092 and DE-SC0007007) and the NSF Division of Information and

501   Intelligent Systems (NSF-1028291). The supercomputing resource is provided by

502   Rosen Center for Advanced Computing at Purdue University. We acknowledge Dr.

503   Stephen C. Whalen made the observational CO flux data available to this study. We are

504   also grateful to University of Tuscia (dep. DIBAF), Italy, and their affiliated members, for

505   their help and the use of their field data.

References:

Badr, O., & Probert, S. D.:Carbon monoxide concentration in the Earth's atmosphere. Applied Energy, doi:10.1016/0306-2619(94)90035-3,1994

Badr, O., & Probert, S. D.: Sinks and environmental impacts for atmospheric carbon monoxide, Applied Energy. doi:10.1016/0306-2619(95)98803-A,1995

Bartholemew, G.W., Alexander, M.: Soils as a sink for atmospheric carbon monoxide, Science 212, 1389-1391, doi:10.1126/science.212.4501.1389, 1981

Bartholomew, G. W., & Alexander, M.: Notes. Microorganisms responsible for the oxidation of carbon monoxide in soil. Environmental Science & Technology. American Chemical Society (ACS), doi:10.1021/es00099a013, 1982

Bender, M., & Conrad, R.: Microbial oxidation of methane, ammonium and carbon monoxide, and turnover of nitrous oxide and nitric oxide in soils, Biogeochemistry, Springer Nature, doi:10.1007/bf00002813, 1994

Bergamaschi, P., Hein, R., Heimann, M., & Crutzen, P. J.: Inverse modeling of the global CO cycle: 1. Inversion of CO mixing ratios, Journal of Geophysical Research: Atmospheres, doi:10.1029/1999jd900818, 2000

Bonan, G.: A Land Surface Model (LSM Version 1.0) for Ecological, Hydrological, and Atmospheric Studies: Technical Description and User's Guide, UCAR/NCAR, doi:10.5065/d6df6p5x, 1996

Bourgeau-Chavez, L.L., Garwood, G.C., Riordan, K., Koziol, B.W., Slawski, J.,: Development of calibration algorithms for selected water content reflectometry probes for burned and nonburned organic soils of Alaska. Int. J. Wildland Fire 19, 961e975, doi:10.1071/wf07175, 2012

Bruhn, D., Albert, K. R., Mikkelsen, T. N., & Ambus, P.: UV-induced carbon monoxide emission from living vegetation. Biogeosciences, Copernicus GmbH, doi:10.5194/bg-10-7877-2013, 2013

Castellanos, P., Marufu, L. T., Doddridge, B. G., Taubman, B. F., Schwab, J. J., Hains, J. C., … Dickerson, R. R.: Ozone, oxides of nitrogen, and carbon monoxide during pollution events over the eastern United States: An evaluation of emissions and vertical mixing, Journal of Geophysical Research Atmospheres, 116(16), doi:10.1029/2010JD014540, 2011

Chan, A. S. K., & Steudler, P. A.: Carbon monoxide uptake kinetics in unamended and long-term nitrogen-amended temperate forest soils. FEMS Microbiology Ecology, 57(3), 343–354, doi:10.1111/j.1574-6941.2006.00127.x, 2006

Conrad, R., & Seiler, W.: Role of Microorganisms in the Consumption and Production of Atmospheric Carbon Monoxide by Soil. Appl. Environ, Microbiol., 40(3), 437–445. Retrieved from http://aem.asm.org/cgi/content/abstract/40/3/437, 1980

Conrad, R., & Seiler, W.: Arid soils as a source of atmospheric carbon monoxide, Geophysical Research Letters, doi:10.1029/gl009i012p01353, 1982

541 Conrad, R., & Seiler, W.: Characteristics of abiological carbon monoxide formation from soil organic
542 matter, humic acids, and phenolic compounds, Environmental Science & Technology, American Chemical
543 Society (ACS), doi:10.1021/es00142a004, 1985

544 Conrad, R., Meyer, O., & Seiler, W.: Role of carboxydobacteria in consumption of atmospheric carbon
545 monoxide by soil, Applied and Environmental Microbiology, 42(2), 211–215, 1981

546 Crutzen, P. J., & Giedel, L. T.: A two-dimensional photochemical model of the atmosphere. 2: The
547 tropospheric budgets of anthropogenic chlorocarbons CO, CH4, CH3Cl and the effect of various NOx
548 sources on tropospheric ozone, J. Geophys. Res., 88(Cll), 6641–6661. doi:10.1029/JC088iC11p06641,
549 1983

550 Crutzen, P.J.: Role of the tropics in atmospheric chemistry, The Geophysiology of Amazonia Vegetation
551 Climate Interaction (Dickinson RE, ed.), pp 107–131. John Wiley, New York, 1987

552 Daniel, J. S., & Solomon, S.: On the climate forcing of carbon monoxide, Journal of Geophysical
553 Research-Atmospheres, 103(D11), 13249–13260. doi:10.1029/98JD00822, 1988

554 Dee, D. P., Uppala, S. M., Simmons, A. J., Berrisford, P., Poli, P., Kobayashi, S., … Vitart, F.: The ERA-
555 Interim reanalysis: configuration and performance of the data assimilation system, Quarterly Journal of
556 the Royal Meteorological Society, doi:10.1002/qj.828, 2011

557 Dentener, F., Drevet, J., Lamarque, J. F., Bey, I., Eickhout, B., Fiore, A. M., … Wild, O.: Nitrogen and
558 sulfur deposition on regional and global scales: A multimodel evaluation, Global Biogeochemical
559 Cycles, 20(4), doi:10.1029/2005GB002672, 2006

560 Derendorp, L., Quist, J. B., Holzinger, R., & Röckmann, T.: Emissions of H2 and CO from leaf litter of
561 Sequoiadendron giganteum, and their dependence on UV radiation and temperature, Atmospheric
562 Environment, 45(39), 7520–7524. doi:10.1016/j.atmosenv.2011.09.044, 2011

563 Duan, Q. Y., Gupta, V. K., & Sorooshian, S.: Shuffled complex evolution approach for effective and
564 efficient global minimization, Journal of Optimization Theory and Applications, 76(3), 501–521.
565 doi:10.1007/BF00939380, 1993

566 Duggin, J. A., & Cataldo, D. A.: The rapid oxidation of atmospheric CO to CO2 by soils, Soil Biology and
567 Biochemistry, 17(4), 469–474, doi:10.1016/0038-0717(85)90011-2, 1985

568 Emmons, L. K., Walters, S., Hess, P. G., Lamarque, J.-F., Pfister, G. G., Fillmore, D., … Kloster, S.:
569 Description and evaluation of the Model for Ozone and Related chemical Tracers, version 4 (MOZART-
570 4), Geoscientific Model Development, 3(1), 43–67. doi:10.5194/gmd-3-43-2010, 2010

571 Fenchel, T., King, G. M., & Blackburn, T. H.: Bacterial biogeochemistry: the ecophysiology of mineral
572 cycling, Bacterial biogeochemistry (p. 307 pp). doi:10.1016/B978-0-12-415836-8.00012-8, 1988

573 Ferenci, T., Strom, T., & Quayle, J. R.: Oxidation of carbon monoxide and methane by Pseudomonas
574 methanica, Journal of General Microbiology, 91(1), 79–91. doi:10.1099/00221287-91-1-79, 1975

575 Fisher, M. E.: Soil-atmosphere Exchange of Carbon Monoxide in Forest Stands Exposed to Elevated and
576 Ambient CO2 (Doctoral dissertation), 2003

577   Fraser, W. T., Blei, E., Fry, S. C., Newman, M. F., Reay, D. S., Smith, K. A., & McLeod, A. R.: Emission of
578   methane, carbon monoxide, carbon dioxide and short-chain hydrocarbons from vegetation foliage under
579   ultraviolet irradiation, Plant, Cell and Environment, 38(5), 980–989. doi:10.1111/pce.12489, 2015

580   Funk, D. W., Pullman, E. R., Peterson, K. M., Crill, P. M., & Billings, W. D.: Influence of water table on
581   carbon dioxide, carbon monoxide, and methane fluxes from Taiga Bog microcosms, Global Biogeochem.
582   Cycles, 8(3), 271–278. doi:10.1029/94gb0122, 1994

583   Galbally, I., Meyer, C. P., Wang, Y. P., & Kirstine, W.: Soil-atmosphere exchange of CH4, CO, N2O and
584   NOx and the effects of land-use change in the semiarid Mallee system in Southeastern Australia, Global
585   Change Biology, 16(9), 2407–2419, doi:10.1111/j.1365-2486.2010.02161.x, 2010

586   Gille, J.: MOPITT Gridded Monthly CO Retrievals (Near and Thermal Infrared Radiances) - Version 6
587   [Data set], NASA Langley Atmospheric Science Data Center. doi:10.5067/TERRA/MOPITT/DATA301,
588   2013

589   Gödde, M., Meuser, K., & Conrad, R.: Hydrogen consumption and carbon monoxide production in soils
590   with different properties, Biology and Fertility of Soils, 32(2), 129–134, doi:10.1007/s003740000226, 2000

591   Guthrie, P. D.: The CH4- CO - OH conundrum: A simple analytic approach, Global Biogeochemical
592   Cycles, doi:10.1029/gb003i004p00287, 1989

593   Hardy, K. R., & King, G. M.: Enrichment of High-Affinity CO Oxidizers in Maine Forest Soil. Applied and
594   Environmental Microbiology, 67(8), 3671–3676, doi:10.1128/AEM.67.8.3671-3676.2001, 2001

595   Harris, I., Jones, P. D., Osborn, T. J., & Lister, D. H.: Updated high-resolution grids of monthly climatic
596   observations - the CRU TS3.10 Dataset, International Journal of Climatology, doi:10.1002/joc.3711, 2013

597   He, H., & He, L.: The role of carbon monoxide signaling in the responses of plants to abiotic
598   stresses, Nitric Oxide : Biology and Chemistry / Official Journal of the Nitric Oxide Society, 42, 40–3.
599   doi:10.1016/j.niox.2014.08.011, 2014

600   Heichel, G. H.: Removal of Carbon Monoxide by Field and Forest Soils1, Journal of Environment Quality,
601   American Society of Agronomy, doi:10.2134/jeq1973.00472425000200040001x, 1973

602   Jobbagy, E. G., & Jackson, R.: The vertical Distribution of soil organic carbon and its relation to climate
603   and vegetation, Ecological Applications, 10:2(April), 423–436, doi:10.2307/2641104, 2000

604   Jones, R. D., & Morita, R. Y.: Carbon monoxide oxidation by chemolithotrophic ammonium
605   oxidizers, Canadian Journal of Microbiology, 29(11), 1545–1551, doi:10.1139/m83-237, 1983

606   Khalil, M. A. ., Pinto, J. ., & Shearer, M.: Atmospheric carbon monoxide, Chemosphere - Global Change
607   Science, Elsevier BV, doi:s1465-9972(99)00053-7,1999

608   Khalil, M. A. K., & Rasmussen, R. A.: The global cycle of carbon monoxide: Trends and mass
609   balance, Chemosphere, 20(1–2), 227–242, doi:10.1016/0045-6535(90)90098-E, 1990

610   King, G. M.: Attributes of Atmospheric Carbon Monoxide Oxidation by Maine Forest Soils, Appl. Environ.
611   Microbiol., 65(12), 5257–5264, 1999

King, G. M.: Characteristics and significance of atmospheric carbon monoxide consumption by soils, Chemosphere, 1, 53–63, doi:10.1016/S1465-9972(99)00021-5, 1999a

King, G. M.: Land use impacts on atmospheric carbon monoxide consumption by soils, Global Biogeochemical Cycles, 14(4), 1161–1172, doi:10.1029/2000GB001272, 2000

King, G. M., & Crosby, H.: Impacts of plant roots on soil CO cycling and soil-atmosphere CO exchange, Global Change Biology, 8(11), 1085–1093, doi:10.1046/j.1365-2486.2002.00545.x, 2002

King, G. M., & Hungria, M.: Soil-atmosphere CO exchanges and microbial biogeochemistry of CO transformations in a Brazilian agricultural ecosystem, Applied and Environmental Microbiology, 68(9), 4480–4485, doi:10.1128/AEM.68.9.4480-4485.2002, 2002

King, G. M., & Weber, C. F.: Distribution, diversity and ecology of aerobic CO-oxidizing bacteria, Nature Reviews, Microbiology, 5(2), 107–18, doi:10.1038/nrmicro1595, 2007

King, J. Y., Brandt, L. A., & Adair, E. C.: Shedding light on plant litter decomposition: advances, implications and new directions in understanding the role of photodegradation, Biogeochemistry, 111(1–3), 57–81, doi:10.1007/s10533-012-9737-9, 2012

Kisselle, K. W., Zepp, R. G., Burke, R. A., De Pinto, A. S., Bustamante, M. M. C., Opsahl, S., … Viana, L. T.: Seasonal soil fluxes of carbon monoxide in burned and unburned Brazilian savannas, Journal of Geophysical Research Atmospheres, 107(20), doi:10.1029/2001JD000638, 2002

Kuhlbusch, T. A., Zepp, R. G., Miller, W. L., & A BURKE, R.: Carbon monoxide fluxes of different soil layers in upland Canadian boreal forests, Tellus B. Informa UK Limited, doi:10.1034/j.1600-0889.1998.t01-3-00003.x, 1998

Lamarque, J. F., Emmons, L. K., Hess, P. G., Kinnison, D. E., Tilmes, S., Vitt, F., … Tyndall, G. K.: CAM-chem: Description and evaluation of interactive atmospheric chemistry in the Community Earth System Model, Geoscientific Model Development, 5(2), 369–411, https://doi.org/10.5194/gmd-5-369-2012, 2012

Lee, H., Rahn, T., & Throop, H.: An accounting of C-based trace gas release during abiotic plant litter degradation, Global Change Biology, 18(3), 1185–1195, doi:10.1111/j.1365-2486.2011.02579.x, 2012

Logan, J. A., Prather, M. J., Wofsy, S. C., & McElroy, M. B.: Tropospheric chemistry - A global perspective, J. Geophys. Res., doi:10.1029/JC086iC08p07210, 1981

Lu, Y., & Khalil, M. A. K.: Methane and carbon monoxide in OH chemistry: The effects of feedbacks and reservoirs generated by the reactive products, Chemosphere. Elsevier BV, doi:10.1016/0045-6535(93)90450-j, 1993

Luo, M., Read, W., Kulawik, S., Worden, J., Livesey, N., Bowman, K., & Herman, R.: Carbon monoxide (CO) vertical profiles derived from joined TES and MLS measurements, Journal of Geophysical Research Atmospheres, 118(18), 10601–10613, doi:10.1002/jgrd.50800, 2013

Moxley, J. M., & Smith, K. A.: Factors affecting utilisation of atmospheric CO by soils, Soil Biology and Biochemistry, 30(1), 65–79, doi:10.1016/S0038-0717(97)00095-3, 1998

647 Myhre, G., Shindell, D., Bréon, F. M., Collins, W., Fuglestvedt, J., Huang, J., ... & Nakajima, T.:
648 Anthropogenic and Natural Radiative Forcing. In: Climate Change 2013: The Physical Science Basis,
649 Contribution of Working Group 1 to the Fifth Assessment Report of the Intergovernmental Panel on
650 Climate Change. Table, 8, 714, 2013

651 Nakai, T., Kim, Y., Busey, R. C., Suzuki, R., Nagai, S., Kobayashi, H., … Ito, A.: Characteristics of
652 evapotranspiration from a permafrost black spruce forest in interior Alaska. Polar Science, 7(2), 136–148.
653 doi:10.1016/j.polar.2013.03.003, 2013

654 Philip, R., & Novick, K.: AmeriFlux US-MMS Morgan Monroe State Forest [Data set]. AmeriFlux; Indiana
655 University, doi:10.17190/AMF/1246080, 2016

656 Pihlatie, M., Rannik, Ü., Haapanala, S., Peltola, O., Shurpali, N., Martikainen, P. J., … Mammarella, I.:
657 Seasonal and diurnal variation in CO fluxes from an agricultural bioenergy crop, Biogeosciences.
658 Copernicus GmbH, doi:10.5194/bg-13-5471-2016, 2016

659 Potter, C. S., Klooster, S. A., & Chatfield, R. B.: Consumption and production of carbon monoxide in soils:
660 A global model analysis of spatial and seasonal variation, Chemosphere, 33(6), 1175–1193,
661 doi:10.1016/0045-6535(96)00254-8, 1996

662 Prather, M., and Ehhalt, D.: Atmospheric chemistry and greenhouse gases. Climate Change, 2001: The
663 Scientific Basis (Houghton JT, Ding Y, Griggs DJ, Noguer M, van der Linden PJ, Dai X, Maskell K &
664 Johnson CA, eds), pp. 239–288, Cambridge University Press, Cambridge, UK, 2001

665 Prather, M., Derwent, R., Ehhalt, D., Fraser, P., Sanheeza, E. and Zhou, X.: Other trace gases and
666 atmospheric chemistry, Climate Change, 1994. Radiative Forcing of Climate Change (Houghton JT, Meira
667 Filho LG, Bruce J, Hoesung Lee BA, Callander E, Haites E, Harris N & Maskell K, eds), pp. 76–126,
668 Cambridge University Press, Cambridge, UK, 1995

669 SALESKA, S. R., DA ROCHA, H. R., HUETE, A. R., NOBRE, A. D., ARTAXO, P. E., & SHIMABUKURO,
670 Y. E.: LBA-ECO CD-32 Flux Tower Network Data Compilation, Brazilian Amazon: 1999-2006, ORNL
671 Distributed Active Archive Center, doi:10.3334/ORNLDAAC/1174, 2013

672 Sanderson, M. G., Collins, W. J., Derwent, R. G., & Johnson, C. E.: Simulation of global hydrogen levels
673 using a Lagrangian three-dimensional model, Journal of Atmospheric Chemistry, 46(1), 15–28,
674 doi:10.1023/A:1024824223232, 2003

675 Sanhueza, E., Dong, Y., Scharffe, D., Lobert, J. M., & Crutzen, P. J.: Carbon monoxide uptake by
676 temperate forest soils: The effects of leaves and humus layers, Tellus, Series B: Chemical and Physical
677 Meteorology, 50(1), 51–58, doi:10.1034/j.1600-0889.1998.00004.x, 1998

678 Schade, G. W., & Crutzen, P. J.: CO emissions from degrading plant matter (II). Estimate of a global
679 source strength, Tellus, Series B: Chemical and Physical Meteorology, 51(5), 909–918,
680 doi:10.1034/j.1600-0889.1999.t01-4-00004.x, 1999

681 Scharffe, D., Hao, W. M., Donoso, L., Crutzen, P. J., & Sanhueza, E.: Soil fluxes and atmospheric
682 concentration of CO and CH4 in the northern part of the Guayana shield, Venezuela, Journal of
683 Geophysical Research-Atmospheres, 95(90), 22475–22480, doi:10.1029/JD095iD13p22475, 1990

Seiler, W.: In: Krumbein, W.E. (Ed.), Environmental Biogeochemistry and Geomicrobiology, Methods, Metals and Assessment, vol. 3, Ann Arbor Science, Ann Arbor, MI, pp. 773-810, 1987

Seinfeld, J. H., & Pandis, S. N.: Atmospheric Chemistry and Physics: From Air Pollution to Climate Change, Atmospheric Chemistry and Physics from Air Pollution to Climate Change Publisher New York NY Wiley 1998 Physical Description Xxvii 1326 p A WileyInterscience Publication ISBN 0471178152, 51, 1–4, doi:10.1080/00139157.1999.10544295, 1998

Stein, O., Schultz, M. G., Bouarar, I., Clark, H., Huijnen, V., Gaudel, A., … Clerbaux, C.: On the wintertime low bias of Northern Hemisphere carbon monoxide found in global model simulations, Atmospheric Chemistry and Physics, 14(17), 9295–9316, doi:10.5194/acp-14-9295-2014, 2014

Stevenson, D. S., Dentener, F. J., Schultz, M. G., Ellingsen, K., van Noije, T. P. C., Wild, O., … Szopa, S.: Multimodel ensemble simulations of present-day and near-future tropospheric ozone, Journal of Geophysical Research Atmospheres, 111(8), doi:10.1029/2005JD006338, 2006

Suzuki, R.: AmeriFlux US-Prr Poker Flat Research Range Black Spruce Forest [Data set], AmeriFlux; Japan Agency for Marine-Earth Science and Technology, doi:10.17190/AMF/1246153, 2016

Tan, Z., & Zhuang, Q.: An analysis of atmospheric CH4 concentrations from 1984 to 2008 with a single box atmospheric chemistry model, Atmospheric Chemistry and Physics Discussions, Copernicus GmbH, doi:10.5194/acpd-12-30259-2012, 2012

Tarr, M. a., Miller, W. L., & Zepp, R. G.: Direct carbon monoxide photoproduction from plant matter, Journal of Geophysical Research, 100, 11403, doi:10.1029/94JD03324, 1995

Taylor, J. A., Zimmerman, P. R., & Erickson, D. J.: A 3-D modelling study of the sources and sinks of atmospheric carbon monoxide, Ecological Modelling, 88(1–3), 53–71, doi:10.1016/0304-3800(95)00069-0, 1996

van Asperen, H., Warneke, T., Sabbatini, S., Nicolini, G., Papale, D., & Notholt, J.: The role of photo- and thermal degradation for CO_2 and CO fluxes in an arid ecosystem, Biogeosciences, 12(13), 4161–4174, doi:10.5194/bg-12-4161-2015, 2015

Varella, R. F., Bustamante, M. M. C., Pinto, A. S., Kisselle, K. W., Santos, R. V., Burke, R. A., … Viana, L. T.: Soil fluxes of CO2, CO, NO, and N2O from an old pasture and from native Savanna in Brazil, Ecological Applications, 14(4 SUPPL.), doi:10.1890/01-6014, 2004

Vreman, H. J., Wong, R. J., & Stevenson, D. K.: Quantitating carbon monoxide production from heme by vascular plant preparations in vitro, Plant Physiology and Biochemistry, 49(1), 61–68, doi:10.1016/j.plaphy.2010.09.021, 2011

Wesely, M. L.: Parameterization of surface resistances to gaseous dry deposition in regional-scale numerical models. Atmospheric Environment (1967), Elsevier BV, doi:10.1016/0004-6981(89)90153-4, 1989

Wesely, M., & Hicks, B.: A review of the current status of knowledge on dry deposition. Atmospheric Environment, 34, 2261–2282, doi:10.1016/S1352-2310(99)00467-7, 2000

721 Whalen, S. C., & Reeburgh, W. S.: Carbon monoxide consumption in upland boreal forest soils, Soil
722 Biology and Biochemistry, 33(10), 1329–1338, doi:10.1016/S0038-0717(01)00038-4, 2001

723 Yonemura, S., Kawashima, S., & Tsuruta, H.: Carbon monoxide, hydrogen, and methane uptake by soils
724 in a temperate arable field and a forest, Journal of Geophysical Research, 105(Dll), 14347,
725 https://doi.org/10.1029/1999JD901156, 2000

726 Yoon, J., & Pozzer, A.: Model-simulated trend of surface carbon monoxide for the 2001-2010
727 decade, Atmospheric Chemistry and Physics, 14(19), 10465–10482, doi:10.5194/acp-14-10465-2014,
728 2014

729 Zepp, R. G., Miller, W. L., Tarr, M. A., Burke, R. A., & Stocks, B. J.: Soil-atmosphere fluxes of carbon
730 monoxide during early stages of postfire succession in upland Canadian boreal forests, Journal of
731 Geophysical Research-Atmospheres, 102(D24), 29301–29311, doi:10.1029/97jd01326, 1997

732 Zhuang, Q., McGuire, A. D., Melillo, J. M., Clein, J. S., Dargaville, R. J., Kicklighter, D. W., … Hobbie, J.
733 E.: Carbon cycling in extratropical terrestrial ecosystems of the Northern Hemisphere during the 20th
734 century: A modeling analysis of the influences of soil thermal dynamics, Tellus, Series B: Chemical and
735 Physical Meteorology, 55(3), 751–776, doi:10.1034/j.1600-0889.2003.00060.x, 2003

736 Zhuang, Q., Melillo, J. M., Kicklighter, D. W., Prinn, R. G., McGuire, A. D., Steudler, P. A., … Hu, S.:
737 Methane fluxes between terrestrial ecosystems and the atmosphere at northern high latitudes during the
738 past century: A retrospective analysis with a process-based biogeochemistry model, Global
739 Biogeochemical Cycles, 18(3), doi:10.1029/2004GB002239, 2004

740 Zhuang, Q., Melillo, J. M., McGuire, A. D., Kicklighter, D. W., Prinn, R. G., Steudler, P. A., … Hu, S.: Net
741 emissions of CH4 and CO2 in Alaska: Implications for the region's greenhouse gas budget, Ecological
742 Applications, 17(1), 203–212, doi:10.1890/1051-0761(2007)017[0203:NEOCAC]2.0.CO;2, 2007

743 Zhuang, Q., Romanovsky, V. E., & McGuire, a. D.: Incorporation of a permafrost model into a large-scale
744 ecosystem model: Evaluation of temporal and spatial scaling issues in simulating soil thermal
745 dynamics, Journal of Geophysical Research, 106, 33649, doi:10.1029/2001JD900151, 2001

746 Zhuang, Q., Chen, M., Xu, K., Tang, J., Saikawa, E., Lu, Y., … McGuire, A. D.: Response of global soil
747 consumption of atmospheric methane to changes in atmospheric climate and nitrogen deposition, Global
748 Biogeochemical Cycles, doi:10.1002/gbc.20057, 2013

Table 1. Model parameterization sites for thermal and hydrology modules (site No. 1-4) and for CODM module (site No. 5-13)

No.	Site Name	Location	Vegetation	Driving Climate	Observed Data	Source and Comments
1	Poker Flat Research Range Black Spruce Forest (US_PRR)	147°29'W/65°7'N	Boreal Evergreen Needle Leaf Forests	Site Observation & ERA Interim	Soil Temperature and Moisture of 2011-2014	Suzuki (2016)
2	Morgan Monroe State Forest (US_MMS)	86°25'W/39°19'N	Temperate Deciduous Broadleaf Forests	Site Observation & ERA Interim	Soil Temperature and Moisture of 1999-2014	Philip and Novick (2016)
3	Santarem, Tapajos National Forest (STM_K83)	54°56'W/3°3'S	Tropical Moist Forest	Site Observation & ERA Interim	Soil Temperature and Moisture of 2000-2004	SALESKA et al. (2013)
4	Bananal Island Site (TOC_BAN)	50°08'W/9°49'S	Tropical Forest-Savanna	Site Observation & ERA Interim	Soil Temperature and Moisture of 2003-2006	SALESKA et al. (2013)
5	Eastern Finland (EF)	27°14E/63°9'N	Boreal Grassland	Site Observation & ERA Interim	CO flux of April-November,2011	Pihlatie et.al. (2016)
6	Viterbo, Italy (VI)	11°55'E/42°22'N	Mediterranean Grassland	Site Observation & ERA Interim	CO flux of August, 2013	van Asperen et al. (2015)
7	Brasilia, Brazil (BB)	47°51'W/15°56'S	Tropical Savanna	Site Observation & CRU	CO flux of October 1999 to July 2001	Varella et al. (2004)
8	Orange County, North Carolina (OC)	79°7'W/35°58'N	Temperate Coniferous Forest	AMF_US-Dk3 2002-2003	CO flux of March 2002 to March 2003	Fisher (2003)
9	Tsukuba Science City, Japan (TSC)	140°7'E/36°01'N	Temperate Mixed Forest	Site Observation & ERA Interim	CO flux of July 1996 to September 1997	Yonemura et. al. (2000)
10	Manitoba, Canada (CBS)	96°44'W/56°09'N	Boreal Pine Forest	Site Observation & AMF_CA-Man	CO flux of June-August, 1994	Kuhlbusch et. al (1998)
11	Scotland, U.K. (SUK)	3°12'W/55°51'N	Temperate Deciduous Forests	ERA Interim 1995	CO flux of 1995	Moxley and Smith (1998)
12	Alaska, USA (AUS)	147°41'W/64°52'N	Boreal wetland	CRU 1991	CO flux of Lab Experiment,1991	Funk et al. (1994)
13	Guayana Shield,Bolivar State,Venezuela (GBV)	62°57'W/7°51'N	Tropical Smideciduous Forest	CRU 1985	CO flux of Lab Experiment,1985	Scharffe et al. (1990)

Table 2. Ecosystem-specific parameters in the CODM module[a]

#	Ecosystem Type	k_{CO} ($ul\ CO\ l^{-1}$)	$Vmax$ ($ug\ CO$ $g^{-1}h^{-1}$)	T_{ref} (°C)	$Q10$ (Unitless)	M_{min} ($\frac{v}{v}$)	M_{max} ($\frac{v}{v}$)	M_{opt} ($\frac{v}{v}$)	E_{SOC}	F_{SOC} ($\frac{g}{g}$)	$\frac{Ea_{ref}}{R}$ (K)	PM_{ref} ($\frac{v}{v}$)	PT_{ref} (°C)
1	Alpine Tundra & Polar Desert	36.00	0.78	4.00	1.80	0.10	1.00	0.55	3.00	0.33	7700	0.25	30.00
2	Wet Tundra	36.00	0.70	4.00	1.80	0.25	1.00	0.55	3.00	0.42	7700	0.25	30.00
3	Boreal Forest	27.34	1.18	9.81	1.60	0.15	0.64	0.53	2.98	0.50	8827	0.35	26.99
4	Temperate Coniferous Forest	42.64	2.15	6.90	1.87	0.02	0.96	0.53	2.86	0.50	8404	0.38	31.52
5	Temperate Deciduous Forest	40.16	2.43	8.54	1.51	0.17	0.81	0.51	2.45	0.50	8801	0.35	37.44
6	Grassland	42.41	0.49	11.27	1.65	0.16	0.82	0.51	3.09	0.42	14165	0.24	12.29
7	Xeric Shrublands	8.00	0.30	4.00	1.50	0.10	1.00	0.55	3.00	0.33	7700	0.25	30.00
8	Tropical Forest	45.00	2.00	4.00	1.50	0.10	1.00	0.55	3.80	0.50	14000	0.50	18.00
9	Xeric Woodland	8.00	0.30	4.00	1.50	0.10	1.00	0.55	3.00	0.50	7700	0.25	30.00
10	Temperate Evergreen Broadleaf Forest	40.16	2.43	8.54	1.51	0.17	0.81	0.51	2.45	0.50	8801	0.35	37.44
11	Mediterranean Shrubland	45.00	1.50	4.00	1.50	0.10	1.00	0.55	3.00	0.33	7700	0.25	30.00
**	Largest Potential Value	51.00	11.1	15.00	2.00	0.30	1.00	0.60	3.80	--	15000	0.60	40.00

[a] k_{CO} is the half-saturation constant for soil CO concentration; $Vmax$ is the specific maximum CO oxidation rate; T_{ref} is the reference temperature to account for soil temperature effects on CO consumption; $Q10$ is the an ecosystem-specific Q10 coefficient to account for soil temperature effects on CO consumption; M_{min}, M_{max}, M_{opt} are the minimum, optimum, and maximum volumetric soil moistures of oxidation reaction to account for soil moisture effects on CO consumption; E_{SOC} is an estimated nominal CO production factor, similar as Potter et al. (1996) (10^{-4} mg CO m^{-2} d^{-1} per g SOC m^{-2}); F_{SOC} is a constant fraction of top 20cm SOC compared to total amount of SOC to account for SOC effects on CO production; Ea_{ref}/R is the is the ecosystem-specific activation energy divided by gas constant to account for the reaction rate of production; PM_{ref} is the reference moisture to account for soil temperature effects on CO production; PT_{ref} is the reference temperature to account for soil temperature effects on CO production

755   **Table 3.** Regional soil CO consumption, net flux and production (Tg CO yr^{-1}) during 2000-2013

	South-45S	45S-0	0-45N	45N-North	Global
Consumption	0.22	75.77	91.66	18.90	186.55
Net flux	0.13	59.34	77.17	14.63	151.27
Production	0.09	16.43	14.49	4.27	35.28

756

757

Table 4. Annual total soil CO consumption, net flux and production in different ecosystems during 2000-2013 (E1) and mean CO deposition velocity in different ecosystems during 1901-2013 (E2)

Vegetation Type	Area (10^6 km^2)	Pixels	Consumption (Tg CO yr^{-1})	Net flux (Tg CO yr^{-1})	Production (Tg CO yr^{-1})	Deposition velocity (mm s^{-1})
Alpine Tundra & Polar Desert	5.28	3580	-0.92	-0.69	0.23	0.023
Wet Tundra	5.24	4212	-1.00	-0.42	0.58	0.015
Boreal Forest	12.47	7578	-7.76	-6.01	1.75	0.070
Forested Boreal Wetland	0.23	130	-0.14	-0.09	0.04	0.109
Boreal Woodland	6.48	4545	-2.48	-1.54	0.94	0.036
Non-Forested Boreal Wetland	0.83	623	-0.35	-0.18	0.17	0.029
Mixed Temperate Forest	5.25	2320	-10.49	-9.98	0.51	0.204
Temperate Coniferous Forest	2.49	1127	-3.51	-3.21	0.30	0.185
Temperate Deciduous Forests	3.65	1666	-5.07	-4.83	0.25	0.151
Temperate Forested Wetland	0.15	60	-0.35	-0.35	0.01	0.281
Tall Grassland	3.63	1567	-1.66	-0.65	1.01	0.021
Short Grassland	4.71	2072	-1.05	-0.27	0.78	0.010
Tropical Savanna	13.85	4666	-21.86	-15.88	5.98	0.234
Xeric Shrubland	14.71	5784	-1.95	-1.64	0.31	0.021
Tropical Evergreen Forest	17.77	5855	-85.90	-69.66	16.24	0.879
Tropical Forested Wetland	0.55	178	-3.59	-3.09	0.50	1.154
Tropical Deciduous Forest	4.69	1606	-14.81	-11.78	3.03	0.532
Xeric Woodland	6.85	2387	-8.48	-7.44	1.04	0.246
Tropical Forested Floodplain	0.15	50	-0.89	-0.77	0.12	1.117
Desert	11.61	4170	-0.62	-0.57	0.05	0.008
Tropical Non-forested Wetland	0.06	19	-0.03	-0.02	0.01	0.067
Tropical Non-forested Floodplain	0.36	120	-0.35	-0.24	0.10	0.083
Temperate Non-Forested Weland	0.34	120	-0.33	-0.20	0.14	0.089
Temperate Forested Floodplain	0.10	48	-0.13	-0.12	0.00	0.197
Temperate Non-forested Floodplain	0.10	45	-0.05	-0.03	0.02	0.050
Wet Savanna	0.16	59	-0.39	-0.32	0.07	0.434
Salt Marsh	0.09	35	-0.05	-0.03	0.03	0.035
Mangroves	0.12	38	-0.49	-0.41	0.08	0.809
Temperate Savannas	6.83	2921	-3.83	-3.22	0.61	0.076
Temperate Evergreen Broadleaf	3.33	1268	-7.17	-6.95	0.22	0.252
Mediterranean Shrubland	1.47	575	-0.86	-0.71	0.16	0.100
Total	133.56	59424	-186.55	-151.27	35.28	--

765

Table 5. Sensitivity of global CO consumption, net flux and production (Tg CO yr^{-1}) to changes in atmospheric

CO, soil organic carbon (SOC), precipitation (Prec) and air temperature (AT)

	Baseline	CO +30%	CO -30%	SOC +30%	SOC -30%	Prec +30%	Prec -30%	AT +3°C	AT -3°C
Consumption	-147.65	-164.14	-131.12	-175.37	-119.90	-150.72	-143.50	-190.59	-114.83
Change (%)	0.00	-11.17	11.19	-18.78	18.79	-2.08	2.81	-29.09	22.23
Net flux	-113.65	-130.15	-97.12	-131.18	-96.10	-116.97	-109.32	-144.23	-89.58
Change (%)	0.00	-14.51	14.54	-15.42	15.44	-2.92	3.81	-26.90	21.18
Production	33.99	33.99	33.99	44.19	23.80	33.74	34.17	46.36	25.25
Change (%)	0.00	0.00	0.00	30.00	-30.00	-0.75	0.53	36.39	-25.72

768

769

770

771

772

773

774

775

776

777

778

779

780

781

782

783

784

785

786

787

789 **Table 6.** Correlation coefficients between forcing variables (precipitation (Prec), air temperature (Tair), soil

790 organic carbon (SOC), soil temperature (Tsoil), soil moisture (Msoil) and atmospheric CO (CO air)) and

791 absolute values of consumption, production and net flux for different regions and the globe

		Monthly					Annual				
		North-45°N	45°N-0°	0°-45°S	45°S-South	Global	North-45°N	45°N-0°	0°-45°S	45°S-South	Global
Prec	Consumption	0.91	0.96	0.92	-0.34	0.87	0.65	0.21	0.26	0.13	0.52
	Production	0.91	0.70	0.45	-0.34	0.82	0.63	0.10	0.15	-0.11	0.47
	Net flux	0.91	0.97	0.94	-0.33	0.87	0.65	0.25	0.31	0.32	0.54
Tair	Consumption	0.97	0.98	0.91	0.96	0.95	0.92	0.93	0.88	0.84	0.91
	Production	0.96	0.83	0.72	0.98	0.94	0.92	0.92	0.91	0.95	0.91
	Net Flux	0.97	0.97	0.88	0.90	0.95	0.91	0.92	0.85	0.62	0.91
SOC	Consumption	-0.19	0.07	0.21	-0.01	0.15	0.68	0.90	0.92	0.47	0.92
	Production	-0.19	0.31	0.47	-0.02	0.24	0.72	0.92	0.92	0.50	0.93
	Net Flux	-0.19	0.03	0.14	0.00	0.13	0.67	0.88	0.91	0.38	0.91
Tsoil	Consumption	0.97	0.98	0.92	0.96	0.95	0.94	0.93	0.88	0.85	0.95
	Production	0.97	0.83	0.72	0.98	0.94	0.94	0.92	0.91	0.96	0.95
	Net Flux	0.98	0.97	0.88	0.90	0.95	0.93	0.93	0.86	0.63	0.95
Msoil	Consumption	0.85	0.96	0.92	0.19	0.76	0.03	0.22	0.14	0.26	0.22
	Production	0.85	0.75	0.44	0.14	0.69	-0.02	0.12	0.02	0.05	0.17
	Net Flux	0.84	0.96	0.95	0.25	0.77	0.04	0.26	0.19	0.40	0.24
CO Air	Consumption	-0.66	-0.76	-0.29	0.14	-0.48	0.87	0.88	0.81	0.98	0.91
	Production	-0.70	-0.66	0.08	-0.40	-0.66	-0.36	-0.48	-0.54	-0.44	-0.57
	Net Flux	-0.64	-0.73	-0.35	0.55	-0.41	0.92	0.91	0.88	0.99	0.94

792

793

794

795

796

797

798

799

800

801

802

803
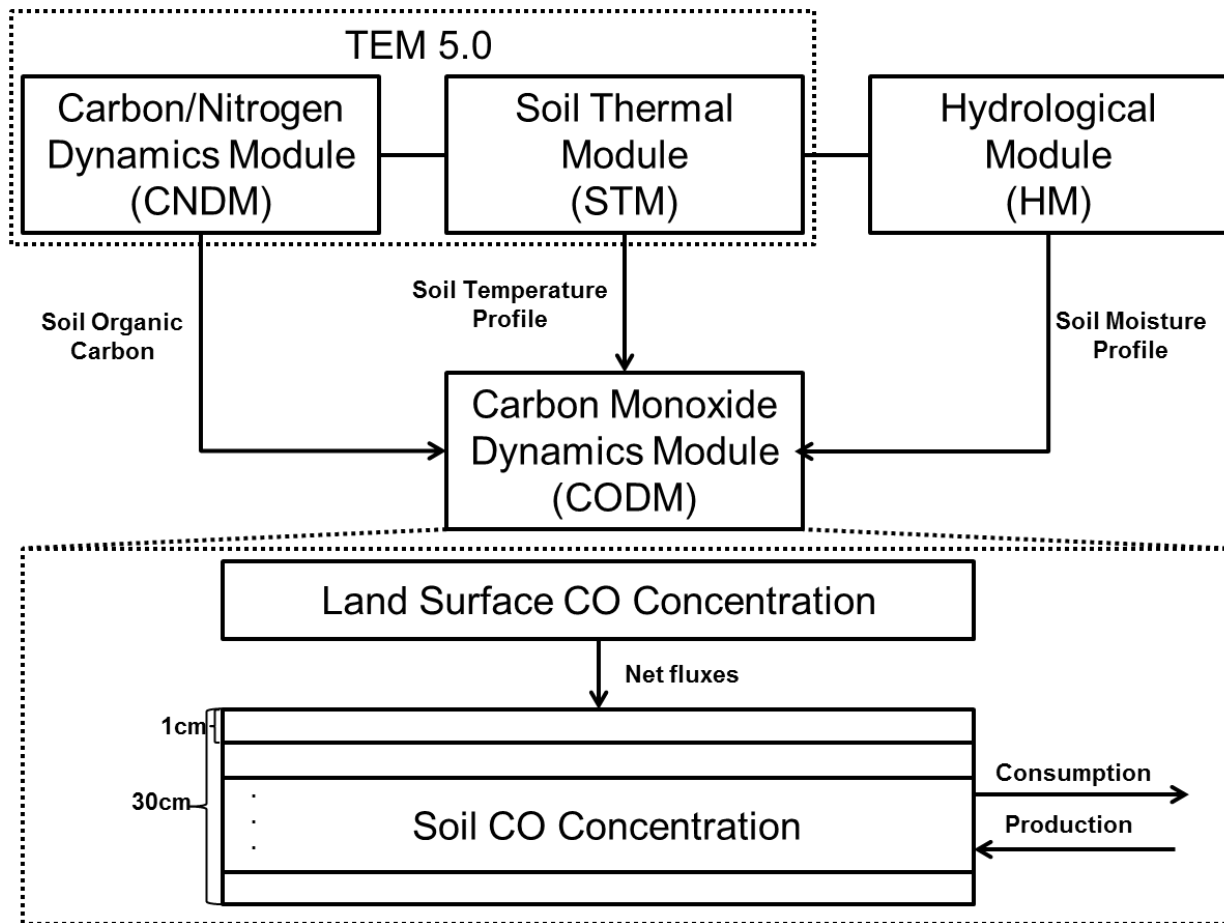
804 **Figure 1. The model framework** includes a carbon and nitrogen dynamics module (CNDM), a soil thermal module (STM)

805 from Terrestrial Ecosystem Model (TEM) 5.0 (Zhuang et al., 2001, 2003), a hydrological module (HM) based on a Land

806 Surface Module (Bonan, 1996; Zhuang et al., 2004), and a carbon monoxide dynamics module (CODM). The detailed

807 structure of CODM includes land surface CO concentration as top boundary and thirty 1 cm thick layers (totally 30 cm)

808 where consumption and production take place.

809

810

811

812

813
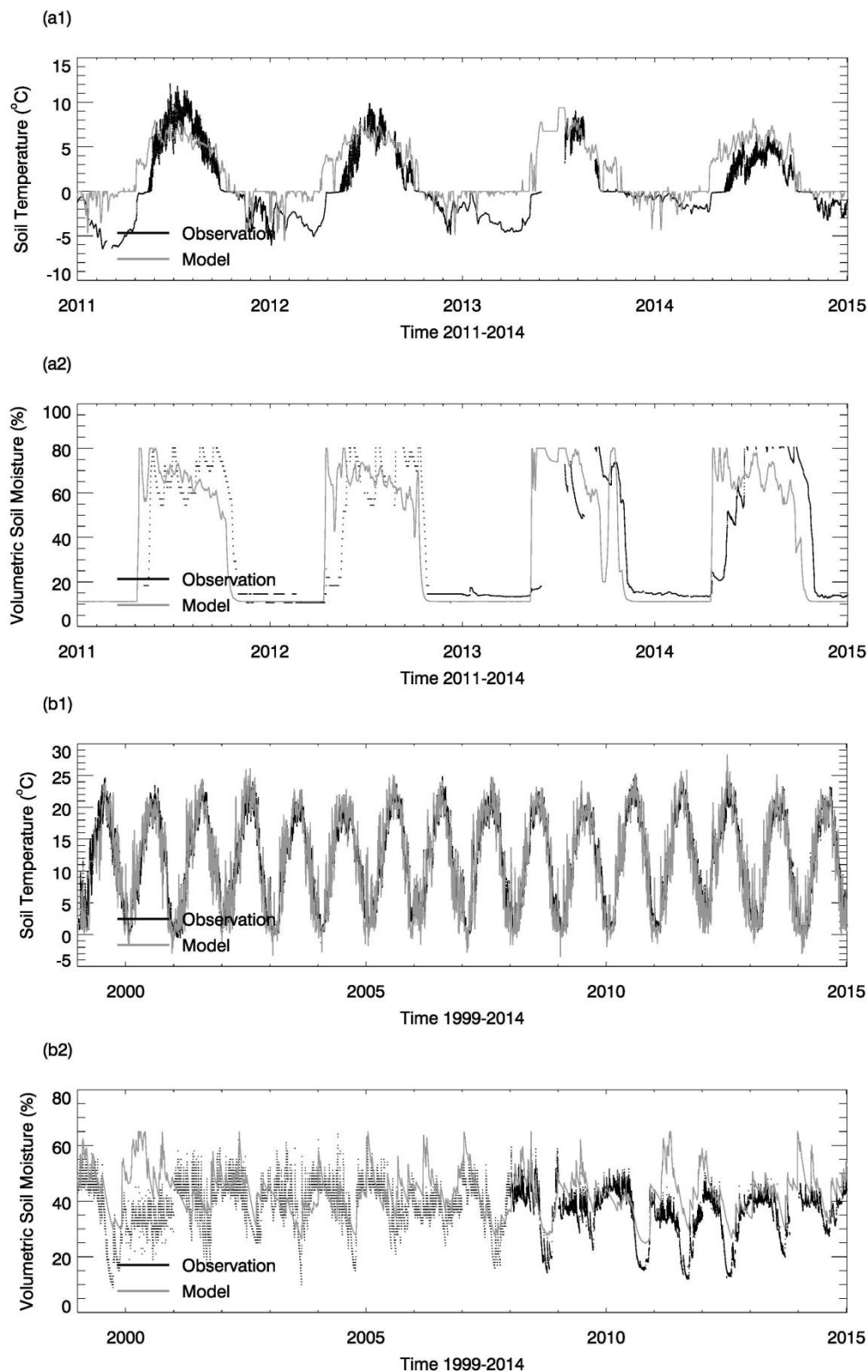
Figure 2. Evaluation of thermal and hydrology module at four sites: (a) Boreal Evergreen Needle Leaf Forests, (b) Temperate Deciduous Broadleaf Forests. (1) shows the soil temperature comparison between model simulations (gray line) and observations (black line) and (2) shows the soil moisture comparison between model simulations (gray line) and observations (black line). Specifically, the volumetric soil moisture is converted from the water content reflectometry (WCR) probe output period using an empirical calibration function of Bourgeau-Chavez et al. (2012) for 5cm-30cm layer. Some of them resulted in calculations of values greater than 100% VSM in Nakai et al. (2013) study. Our model estimated high VSM (close to 80%) is due to top 10 cm moss in the model which has a saturation VSM of 0.8

844
845
846
847
848
849
850
851
852
853
854
855
856
857
858
859
860
861
862
863
864
865
866
867
868
869
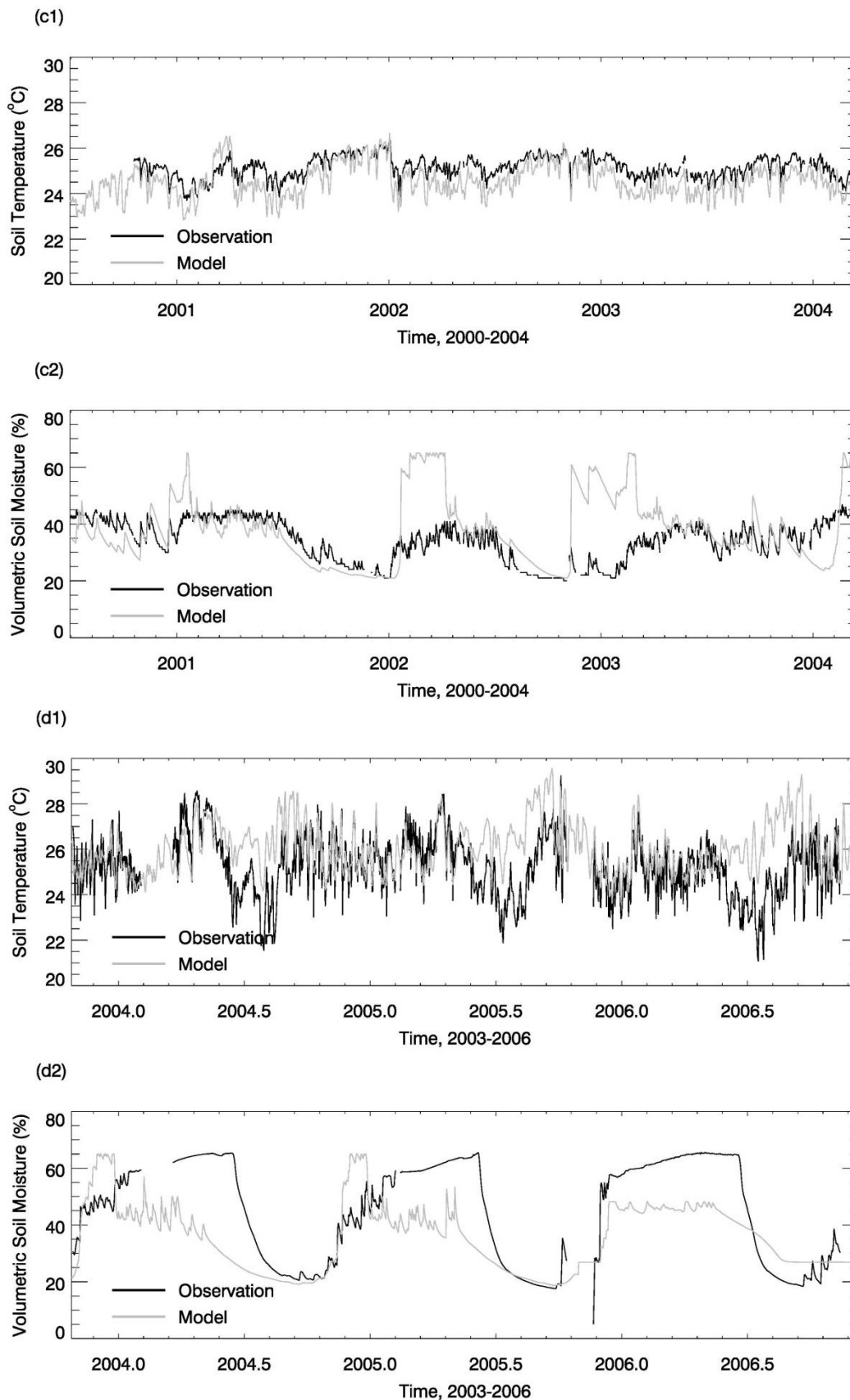
870 **Figure 2. Contd.** Evaluation of thermal and hydrology module at four sites: (c) Tropical Moist Forest, (d) Tropical Forest-
871 Savanna. (1) shows the soil temperature comparison between model simulations (gray line) and observations (black line)
872 and (2) shows the soil moisture comparison between model simulations (gray line) and observations (black line)

Figure 3. Parameter ensemble experiment results: Each parameter has 50 calibrated values generated from running SCE-UA-R 50 times independently. Parameters are normalized to their largest potential values described in Table 2. (a1) and (a2) are temperate coniferous forest normalized parameter distribution boxplots and CO flux comparisons between model simulations (solid line, using mean value of parameters) and observations (green diamond, red lines represent error bar, site No.8), respectively. For each box, line top, box top, horizontal line inside box, box bottom and line bottom represent maximum, third quartile, median, first quartile and minimum of 50 parameter values. Red dot represents the mean value of 50 parameter values. (b1) and (b2) are plots for temperate deciduous forest (site No.11).

Figure 3. Contd. Parameter ensemble experiment results: Each parameter has 50 calibrated values generated from running SCE-UA-R 50 times independently. Parameters are normalized to their largest potential values described in Table 2. (c1) and (c2) are boreal forest normalized parameter distribution boxplots and CO flux comparisons between model simulations (solid line, using mean value of parameters) and observations (green diamond, red lines represent error bar, site No. 12), respectively. For each box, line top, box top, horizontal line inside box, box bottom and line bottom represent maximum, third quartile, median, first quartile and minimum of 50 parameter values. Red dot represents the mean value of 50 parameter values. (d1) and (d2) are for grassland (site No.6). Grassland observation data is the sum of hourly observations so error bar represented the standard deviation.

923

924 **Figure 4.** Historical global land surface (excluding Antarctic area and ocean area) mean climate, and simulated global

925 mean soil moisture, soil temperature and SOC for the period 1901-2013.

926

927
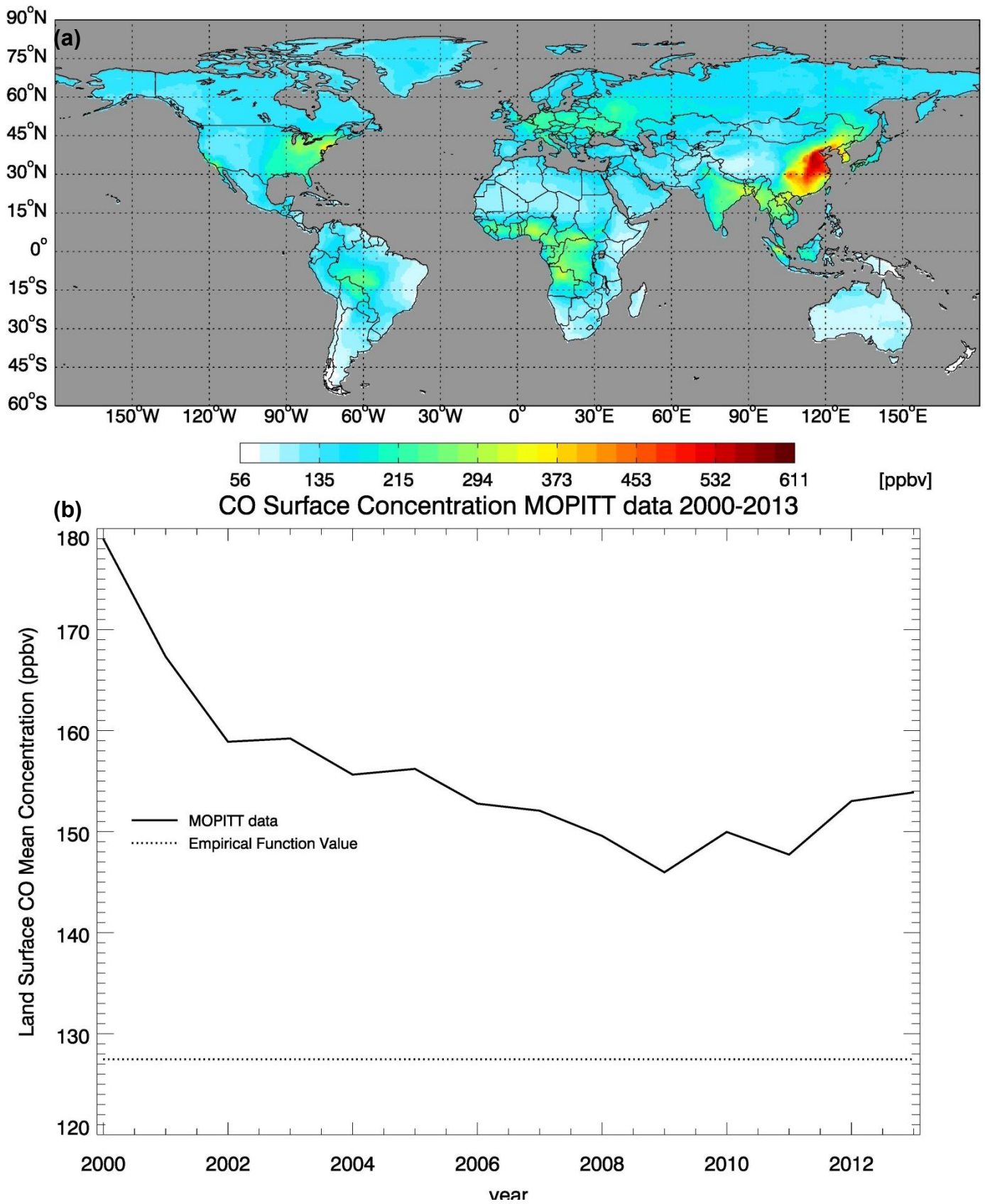
Figure 5. CO surface concentration data from MOPITT satellite (ppbv): (a) global mean CO surface concentrations from MOPITT during 2000-2013; (b) the CO annual surface concentrations from both MOPITT and empirical functions (Potter et al., 1996).
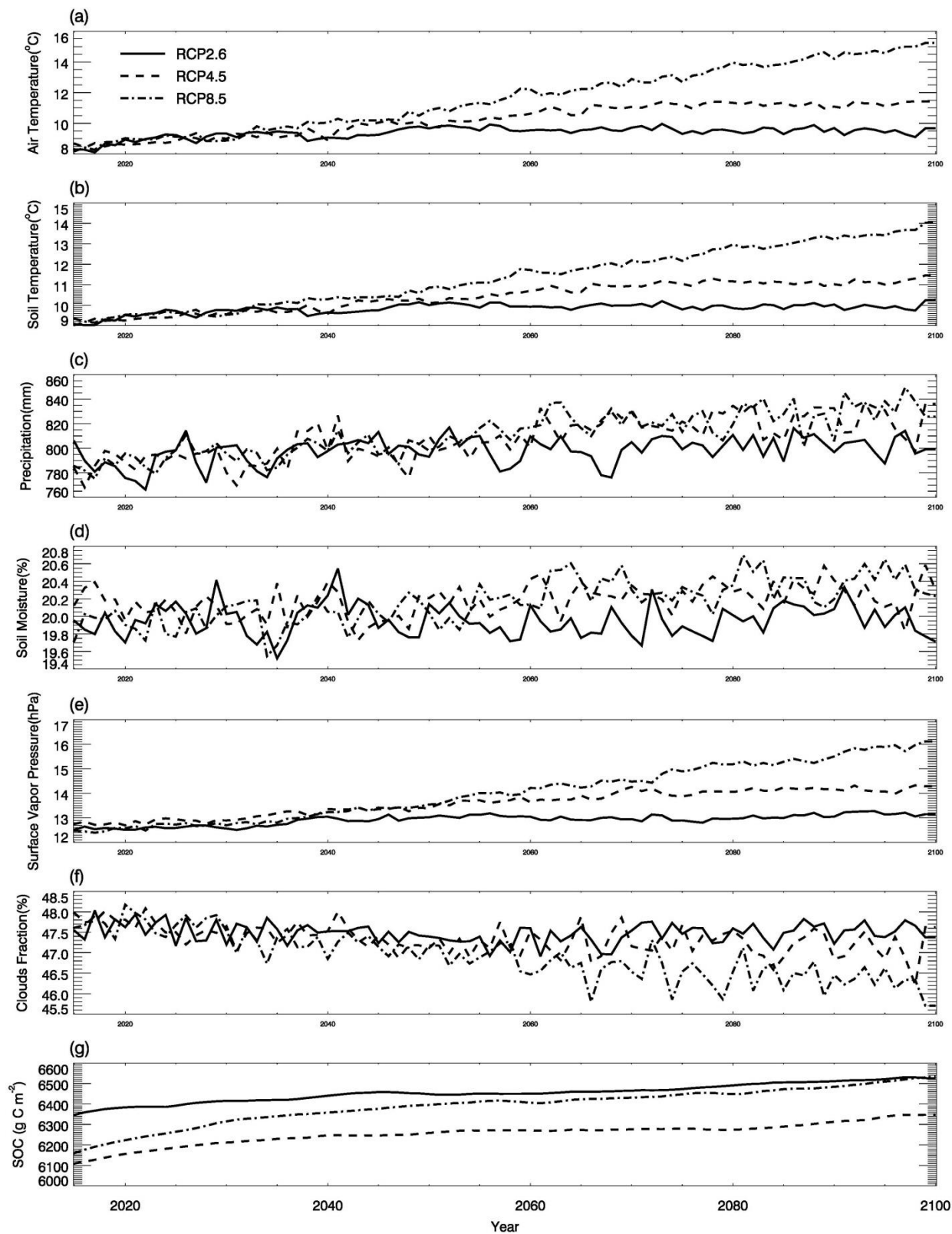
Figure 6. Global land surface (excluding Antarctic area and ocean area) mean climate from RCP2.6, RCP4.5 and RCP8.5 data sets and simulated mean soil temperature, moisture and SOC: (a)-(g) are land surface air temperature (℃), soil temperature (℃), precipitation (mm), soil moisture (%), surface water vapor pressure (hpa), cloud fraction (%), and SOC (mg m^{-2}), respectively.
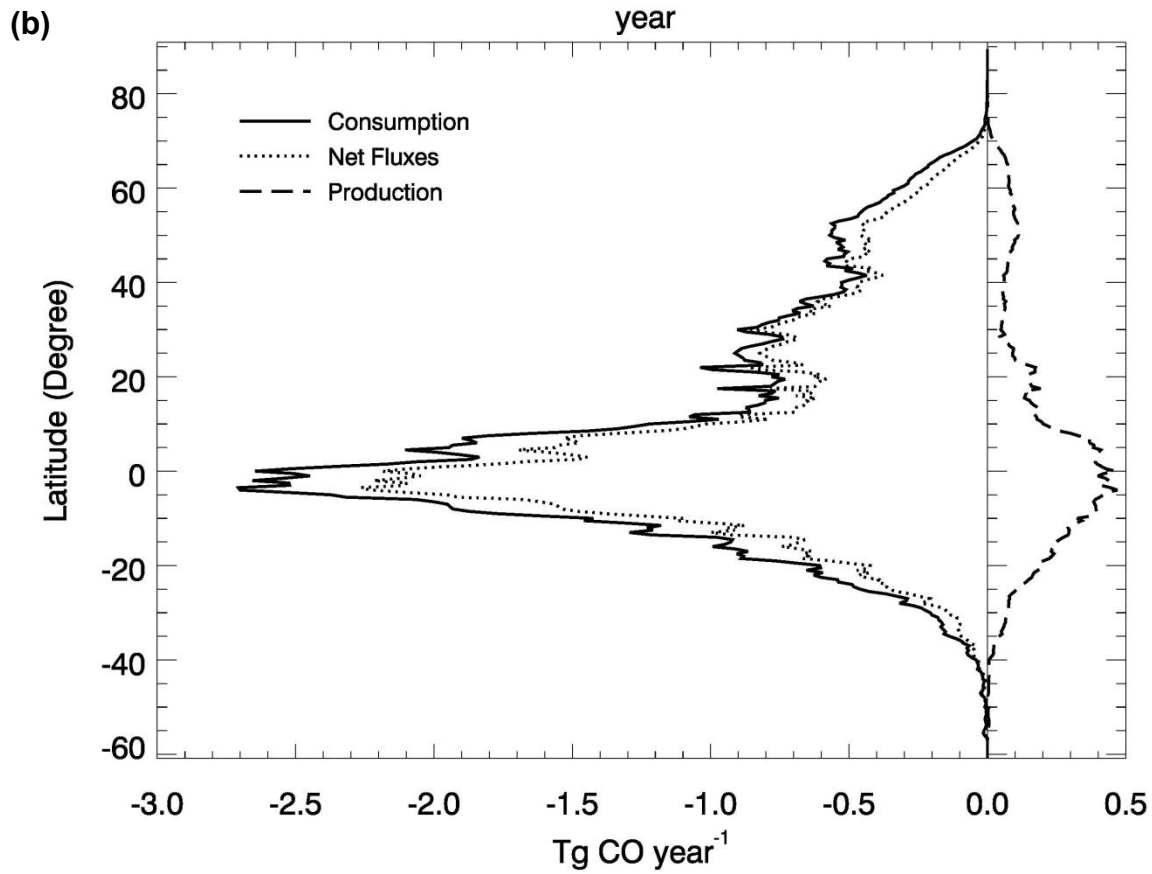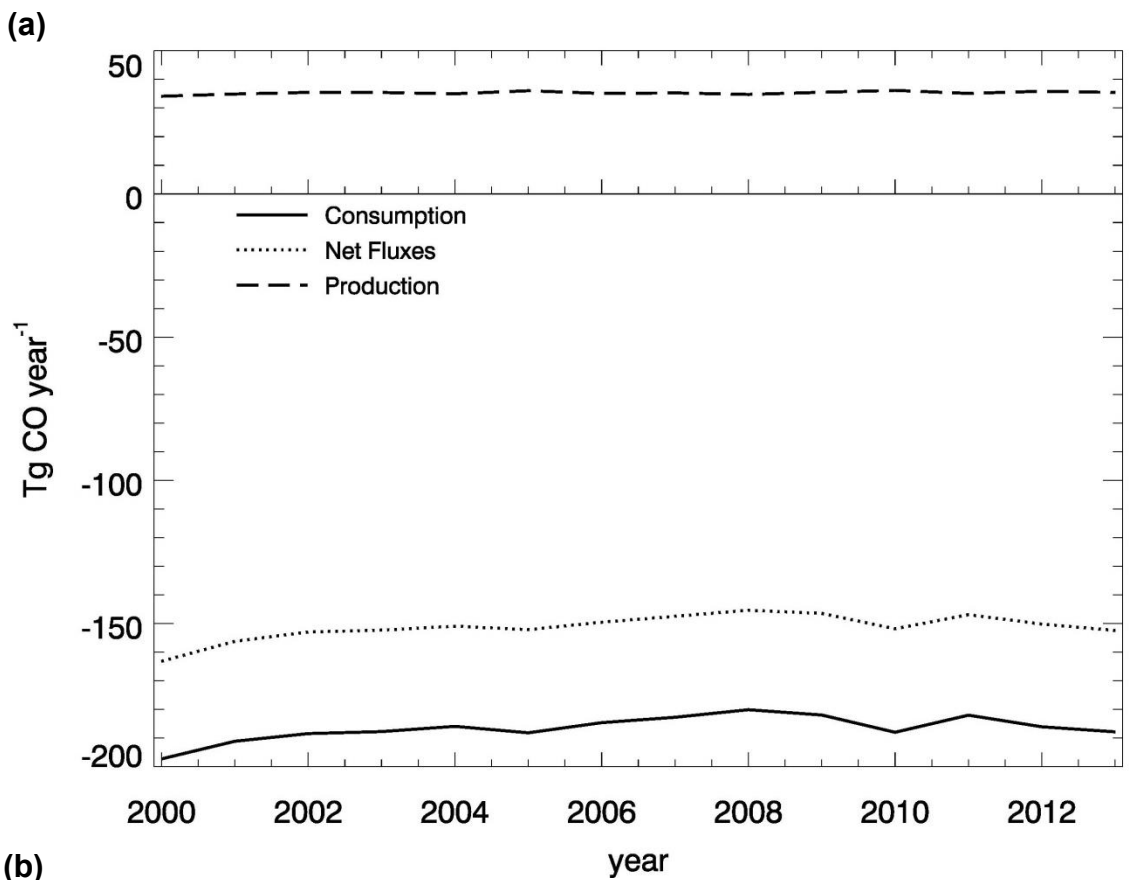
Figure 7. Global mean soil CO consumption, production and net flux: (a) annual time series during 2000-2013and (b) latitudinal distribution during 2000-2013.

014

015
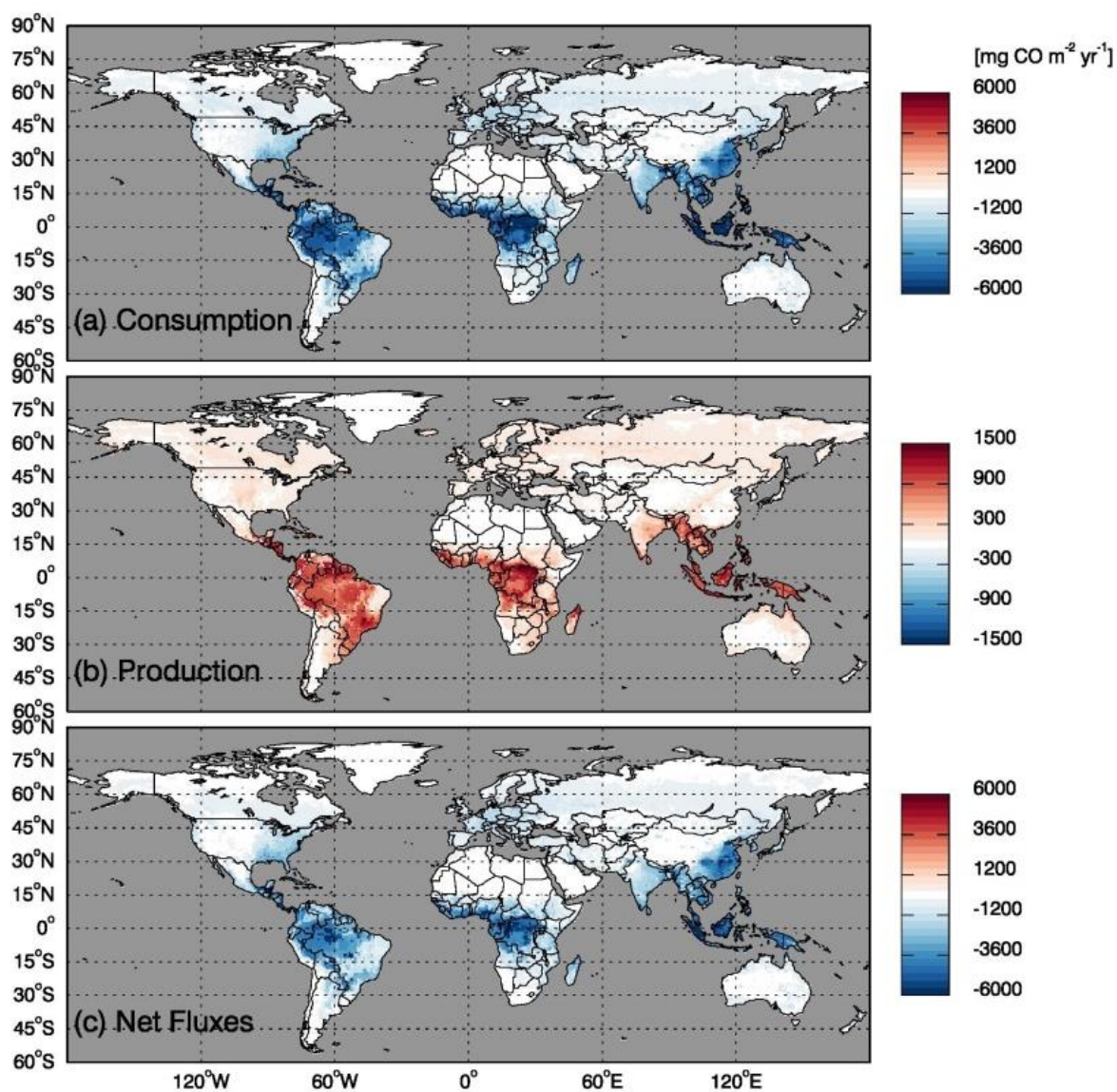
Figure 8. Global annual mean soil CO fluxes (mg CO m^{-2} yr^{-1}) during 2000-2013 using MOPITT CO atmospheric surface concentration data (right side)

016
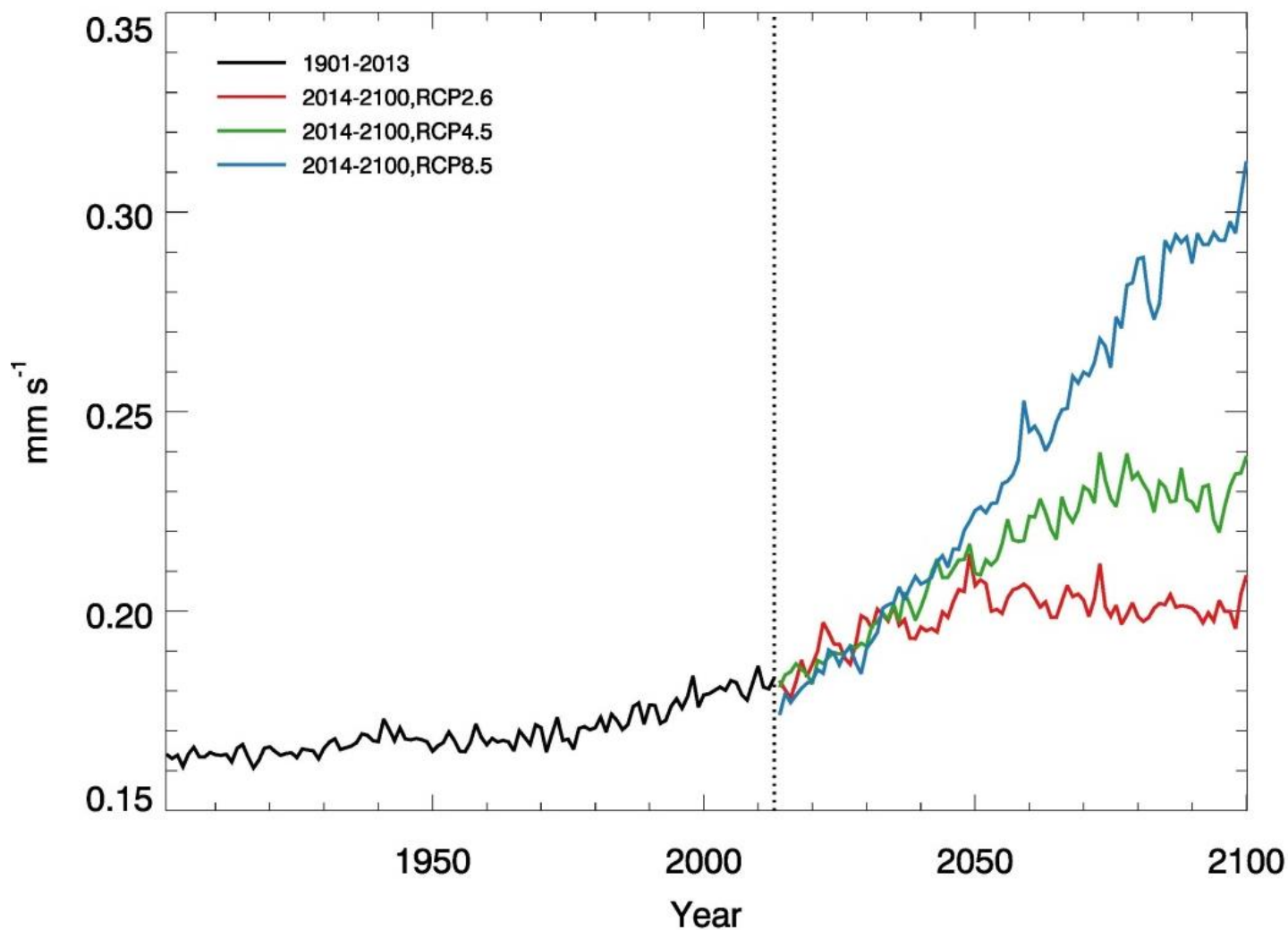
017 **Figure 9.** Future Global mean annual time series of CO deposition velocity (mm s^{-1}) using constant in time,

018 spatially distributed CO concentration data during 1901-2013 (left side of dot line) and under future climate
scenarios RCP2.6, RCP4.5 and RCP8.5 during 2014-2100 (right side of dot line)

019

020
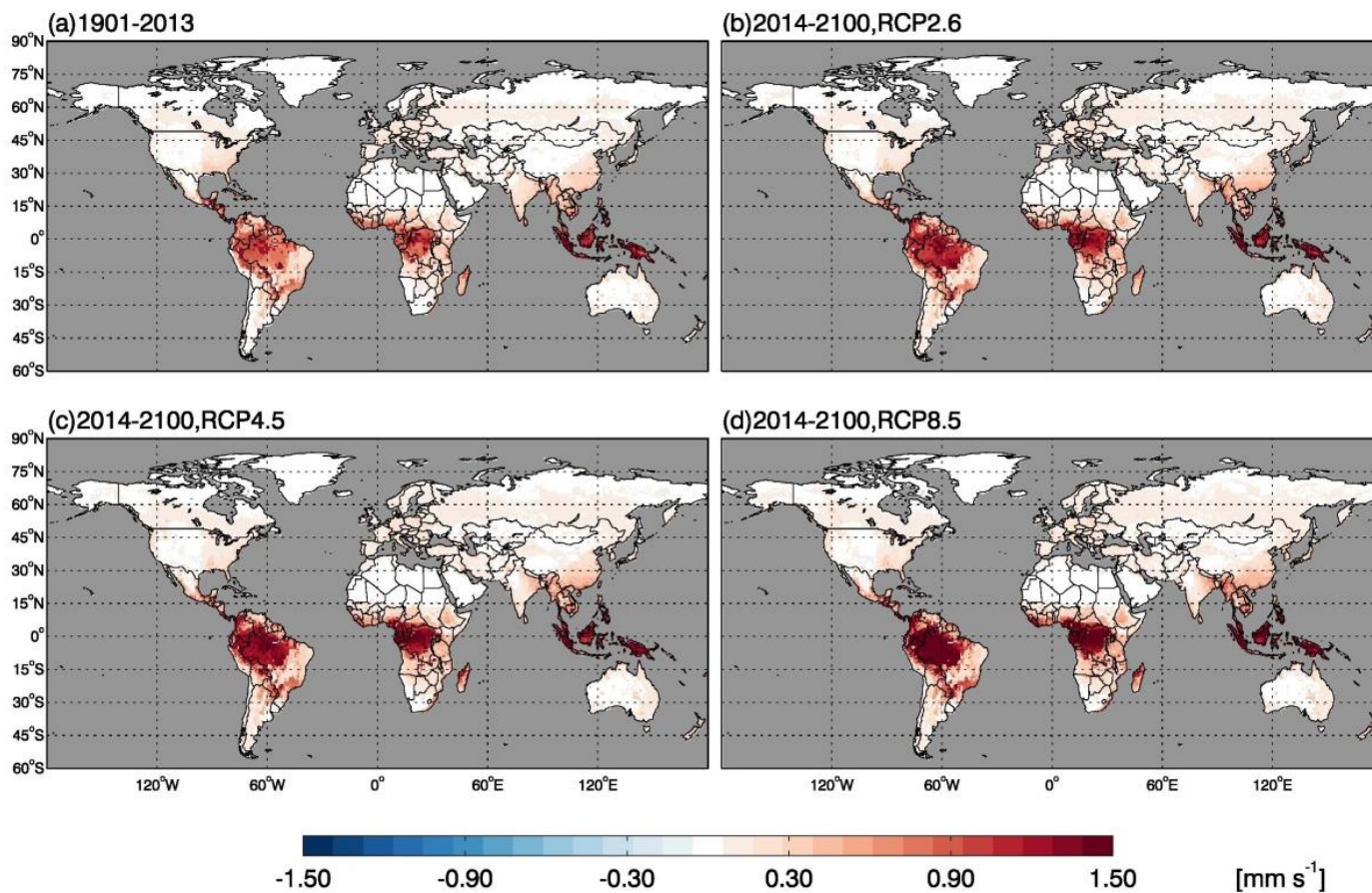
021 **Figure 10.** Global annual mean CO deposition velocity using constant in time, spatially distributed CO
concentration data (mm s^{-1}) a) during 1901-2013 and b), c), d) under future climate scenarios RCP2.6, RCP4.5 and
022 RCP8.5 during 2014-2100, respectively,

023
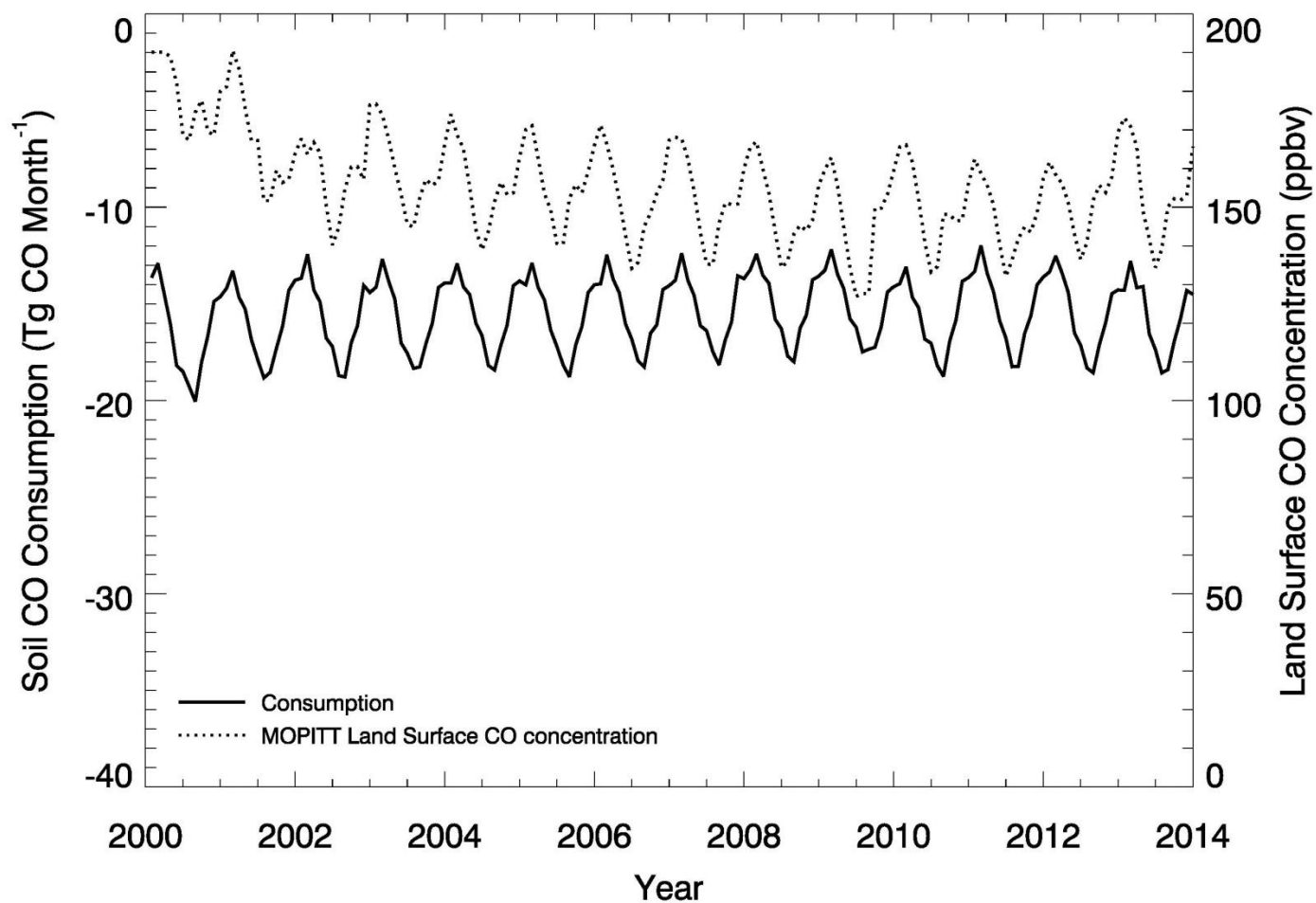
024 **Figure 11.** Global mean monthly time series of MOPITT surface atmospheric CO concentration (ppbv) and soil CO consumption from model simulations E1 (Tg CO mon[-1])

025
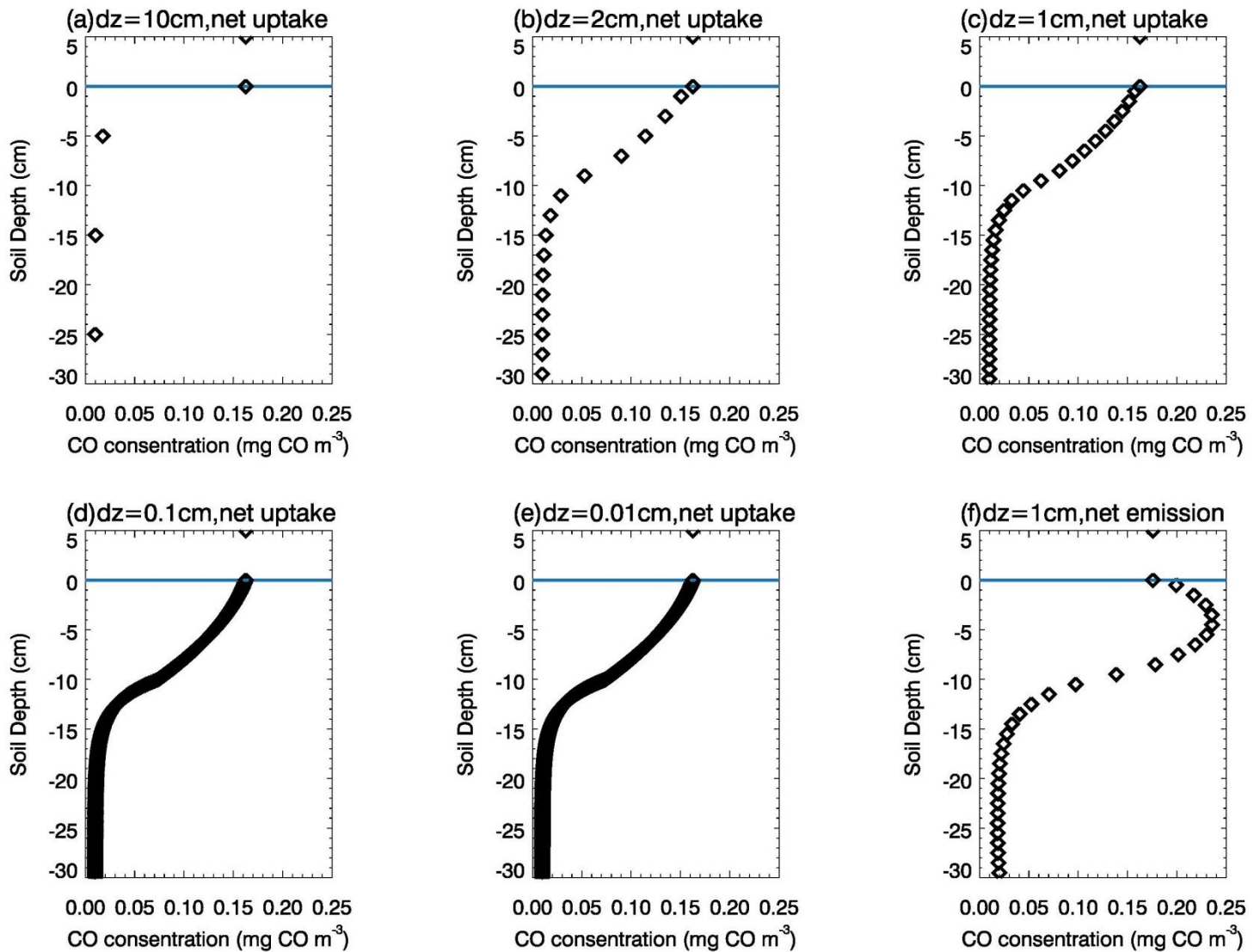
Figure 12. Daily mean vertical soil CO concentration profiles of top 30cm. In soils (depth < 0cm), black diamonds represent the soil CO concentration (mg CO m^{-3}). Above the surface (depth>=0cm), black diamonds represent atmospheric CO concentration. a), b), c), d) and e) are the results from the same day when soil is a net sink of CO but with different layer thickness (dz=10cm, 2cm, 1cm, 0.1cm and 0.01cm respectively); f) is the result from the day when soil is a net source of CO, with dz=1cm.